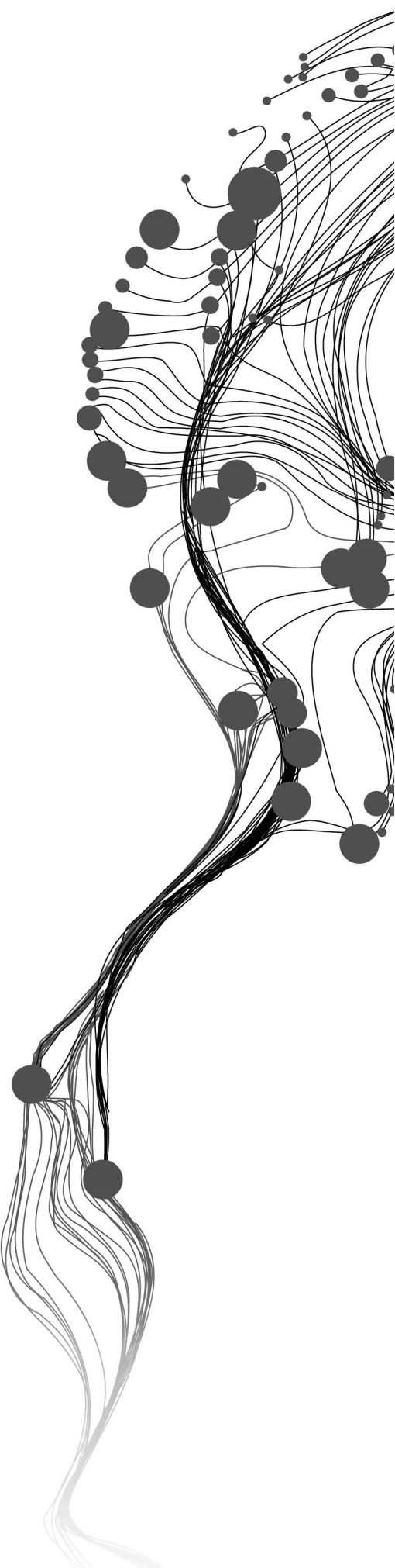


ESTIMATING CHLOROPHYLL-A ABSORPTION AS A PROXY TO PHYTOPLANKTON BIOMASS FROM MERIS DATA LAKE NAIVASHA, KENYA

Mussie Ghirmai
March, 2011

SUPERVISORS:
Dr.Ir. C.M.M. (Chris) Mannaerts
Dr. Ir. Mhd. Suhyb Salama



ESTIMATING CHLOROPHYLL-A ABSORPTION AS A PROXY TO PHYTOPLANKTON BIOMASS FROM MERIS DATA LAKE NAIVASHA, KENYA

Mussie Ghirmai

Enschede, the Netherlands, March, 2011

Thesis submitted to the Faculty of Geo-Information Science and Earth Observation of the University of Twente in partial fulfilment of the requirements for the degree of Master of Science in Geo-information Science and Earth Observation.

Specialization: Water Resources and Environmental Management

SUPERVISORS:

Dr.Ir. C.M.M. (Chris) Mannaerts

Dr. Ir. Mhd. Suhyb Salama

THESIS ASSESSMENT BOARD:

Prof. Dr. Ing. Wouter Verhoef (Chair)

Prof. Dr. M. David Harper (External Examiner, University of Leicester)

Disclaimer

This document describes work undertaken as part of a programme of study at the Faculty of Geo-Information Science and Earth Observation of the University of Twente. All views and opinions expressed therein remain the sole responsibility of the author, and do not necessarily represent those of the Faculty.

ABSTRACT

This paper has investigated chlorophyll-*a* light absorption coefficient in lake Naivasha as a proxy to estimate the phytoplankton biomass using MERIS full resolution (FR) data (300 m) and empirical algorithms. An increase in the phytoplankton content of water bodies contributes to a profound degradation in water quality that can have adverse ecological and human health effects through production of toxins in the presence of cyanobacterias or mechanical damage to marine environment. Since such algal bloom events are sporadic in time and isolated in space, traditional field based measurement and monitoring methods for detecting blooms of phytoplankton are costly and time consuming, delaying management decisions. Remote sensing technique which utilizes the optical properties (absorption and reflectance) of blue-green algal pigments (chlorophyll *a* and phycocyanin) can provide rapid detection of algal blooms. The water leaving reflectance from MERIS FR products were derived using an image based processing (by comparing with the in-situ reflectance) for estimating and correcting atmospheric noise recorded by the sensor. Coupled with physical and bio-chemical data from lakes, remote sensing can provide an efficient method for tracking algal bloom occurrence and their distribution in time and space for long-term management strategies.

A total of about 169 in-situ radiometric and about 137 absorbance spectra were collected during one cruise from 17th of September 2010 to 03rd October 2010 in the two physically interconnected but optically different lakes; the Crescent Island lagoon and the main Lake Naivasha using a Trios RAMSESARC radiance sensor (7° field of view, 320–950 nm), and a Trios RAMSES-ACC-VIS irradiance sensors. Ground truth samples were analyzed for pigment absorption coefficients immediately after sampling using the RD2000 Spectrophotometer.

An atmospheric correction was implemented on the MERIS imagery data and validated using in-situ hyperspectral water leaving reflectance (WLR) spectra measured on Lake Naivasha. The R² and RMSE values between the atmospherically corrected satellite derived WLR and in-situ measured values in the NIR was 0.746 and 0.117 respectively.

Previously published empirical spectral algorithms for the detection of chl-*a* by Gitelson (2008), Shen et al. (2010), and FLH baseline methods by Gower et al. (2004), were applied to the in-situ phytoplankton absorption coefficient, Trios-reflectance and MERIS derived reflectance spectra divided into calibration and validation dataset. To account for weak FLH signal at around 685nm due to the higher chlorophyll content of lake Naivasha, a similar technique known as Maximum Chlorophyll index (MCI) Gower et al. (2005) was analyzed using the 709 nm band peak in the Trios and MERIS reflectance spectrum. Spectral measurements with concurrent analytical laboratory data were analyzed using statistical least square regressions for the determination of best fit coefficients. Algorithm accuracy was tested through a least squares regression by r² and RMSE. Results show that three band algorithm of chl-*a* absorption coefficients prediction yielded coefficients of determination as high as 0.84, RMSE 0.058, for an aggregated dataset (n=42). The SCI and MCI empirical algorithms for the estimation of chl-*a* absorption coefficients resulted in a poor correlation with the in-situ absorption coefficients. A weak polynomial quadratic relationship was found between the SCI and MCI algorithms against the in-situ absorption coefficient (n=42) which is inadequate for characterizing the highly dynamic phytoplankton distribution of lake Naivasha. Although no improvement could be achieved for the poor correlation between the MCI index value and in-situ phytoplankton coefficient, the underperformance of the SCI algorithm showed an increase in the correlation coefficient for stations with SCI index and light absorption values of less than 0.0123sr⁻¹ and 0.02m⁻¹ respectively which is a lower value for lake Naivasha. Result obtained suggests that the three band algorithm is more robust and accurate and was used for mapping the phytoplankton absorption in lake Naivasha.

Keywords: Phytoplankton Biomass; Chlorophyll-*a* absorption; remote sensing; MERIS; Lake Naivasha.

ACKNOWLEDGEMENTS

I would first like to thank the European Space Agency ESA, for providing us MERIS FR level 1b data of lake Naivasha as part of the MERIS validation processes.

I am very grateful to my supervisors, Dr.Ir. C.M.M. Chirs Mannaerts and Dr.Ir. Mhd. Suhyb Salama for their endless guidance, patience, and faith in me. Though it was evident that they were often concerned about the direction in which I was headed, they entertained my every hair brained idea and whim. I am certain that my success as a graduate student has been primarily based on my relationship with them which has far exceeded all of my expectations.

I must also thank to a number of people and organizations who contributed immensely to the successful completion of this study.

Special thanks to Dr. D. M. Harper from University of Leicester, UK for his invaluable contribution in this research for allowing us use his complete and well equipped laboratory in Naivasha with out any limit. Dr. D. M. Harper is grateful not only for his bio-optical laboratory but also for the many scientific researches he has done in the lake.

I would also like to thank Mrs. Sarah Higgins a farmer and environmentalist in Naivasha for her support and encouragement for the work by allowing us to use her Yatch beach gate during entire work period.

I would also like to thank to all who have contributed in some way or the other in this research. Many thanks must also go to Mr. Ruben laboratory technician in the Dr. D. M. Harper laboratory for his friendly encouragement and support in the work. I am also very thankful to my friend Mr. Micheal Ghebru for being my support system, my mentor and confidant during my hard times. Also many thanks to Ms. Eleni Eyob for the free assistance she gave me in collecting data on the lake from the boat.

I am very grateful to my family, relatives and friends back home for their endless love, encouragement and support, and tolerance in actively listening to my endless rants about remote sensing of chlorophyll-a, a topic in which they have never heard of and likely little interest. Special thanks to my parents who have faith in my every decision and who recognize and willingly acknowledge that the outcome won't always be brilliant.

I would also like to thank the WREM department staffs and students of 2009 of the faculty of the Geo-Information Sciences and Earth Observation of the University of Twente for their good spirit, understanding, and tolerance on those days when things were looking less than favourable.

At last but not least the Royal Government of Netherlands must be thanked for allowing me to join the 2009 WREM Msc. Course in ITC and for funding this project through the Netherlands Fellowships Programme (NFP).

TABLE OF CONTENTS

Abstract.....	i
Acknowledgements	ii
Table of contents	iii
List of figures.....	iv
List of tables	v
List of abbreviations	vi
1. INTRODUCTION.....	1
1.1. Research Problem	2
1.2. Research Objectives	3
1.3. Research Questions.....	3
1.4. Research Hypothesis.....	3
1.5. Thesis Outline	3
2. LITRATURE REVIEW.....	5
2.1. Phytoplankton Bloom Distribution in Lake Naivasha.....	5
2.2. Background on Remote Sensing water Quality	5
2.3. Background on Model Types.....	6
3. STUDY AREA MATERIALS and METHODOLOGY	9
3.1. Study Area Description	9
3.2. Sampling and Radiometric Measurement Points Distribution.....	10
3.3. Description of Materials Used.....	11
3.3.1. In-Situ Datasets	11
3.3.2. Remote sensing Datasets.....	11
3.4. Methodology	13
3.4.1. Data Collection.....	14
3.4.2. Data Processing	15
4. DATA ANALYSIS METHOD	21
4.1. Spectral Analysis	21
4.2. Summary of Spectral Reflectance Features Observed.....	21
4.3. Empirical Algorithms used	24
4.3.1. Three Band Algorithm.....	24
4.3.2. Synthetic Chlorophyll Index.....	26
4.3.3. Fluorescence Line Height	28
4.4. Algorithm Calibration and Validation	30
4.5. Measuring Algorithm Accuracy and Robustness	32
5. RESULTS AND DISCUSSION	32
6. CONCLUSSION AND RECCOMMENDATION	39
List of references	40

LIST OF FIGURES

Figure 1. Location map and field measurement ponits distribution.	9
Figure 2. Malewa and Gilgl flood plains, Crescent Island logoon and Main lake water condition.....	10
Figure 3. Schematic representation of the general methodology.	13
Figure 4. Comparison between in-situ and MERIS derived reflectance spectra.	19
Figure 5. Shows spectral features in the reflectance of Trios-sensor measured from lake Naivasha.	22
Figure 6. In situ absorption and corresponding reflectance spectra (left and right)	23
Figure 7. Schematic representation of SCI algorithm.	28
Figure 8. Water reflectance spectra for chlorophyll a concentrations of 0.1, 3, 30 and 300 mgm ⁻³ ,	29
Figure 9 Schematic representation of MCI algorithm.....	30
Figure 10 . Model Calibration with in-situ measured absorption coeffcient.....	31
Figure 11. Validation of the three models against in-situ measured a-phy	33
Figure 12. In-situ absorption coefficient and model index values	36
Figure 13 Phytoplankton absorption maps for the 20th, 23rd and 26th of September 2010.....	37

LIST OF TABLES

Table 1 List of empirical algorithms employed to derive chl-a from lake Naivasha.	8
Table 2 Statistical summary of averaged in-situ measurements	11
Table 3 Summary of earth observation data used in the study.	12
Table 4 Characteristics of MERIS data in Lake Naivasha	12
Table 5 Samples Collected, processed and retained.....	14
Table 6. Calibratoin summary of the three models	32
Table 7 Performance summary of the three band algorithm.	33

LIST OF ABBREVIATIONS

Term	Description
AOP	Apparent optical properties
$a_{\text{phy}}(\lambda)$	Absorption by phytoplankton
$a_{\text{dg}}(\lambda)$	Absorption by gelbistof and detritus
$a_{\text{chl-a}}^*$	Chlorophyll-a Specific Absorption Coefficient
CDOM	Coloured dissolved organic matters
C2P	Case-2 Regional Processor
C2R	Case-2 Regional
[Chl-a]	Chlorophyll-a concentration
Chl-a	Chlorophyll-a
CZCS	Coastal Zone Colour Scanner
ENVISAT	Environmental Satellite
EO	Earth observation
IOCCG	International Ocean Colour Coordinating Group
IOP	Inherent optical properties
MODIS	Moderate Resolution Imaging Spectrometer
MERIS	Medium Resolution Imaging Spectrometer
NIR	Near-InfraRed
NAP	Non-Algal Particle
OC3M	Ocean Chlorophyll 3 MODIS
Rrs	Remote Sensing Reflectance
RS	Remote sensing
RTE	Radiative Transfer Equation
SCI	Synthetic Chlorophyll index
SSC	Suspended Sediment concentration
TSS	Total Suspended Sediment
SeaWiFS	Sea-viewing Wide Field-of-view Sensor
SPM	Suspended particulate matters
TOA	Top of atmosphere
WLR	Water leaving reflectance

1. INTRODUCTION

Algal blooms can result in ecological, social and economic depreciation to lakes and reservoirs by producing surface scum, unpleasant taste and odour to drinking water (from production of metabolites) and possible adverse effects to human health from blue-green algal toxins. These microscopic organisms that live both in fresh and salty water environments are collectively termed as phytoplankton. Derived from the Greek words phyto (plant) and plankton (made to wander or drift), phytoplankton are wandering plants. Like land plants, phytoplankton have chlorophyll to capture sunlight, and use photosynthesis to turn it into chemical energy by consuming carbon dioxide and releasing oxygen. Blooms of phytoplankton can cover hundreds of square kilometres in oceans and lakes and are easily visible in satellite images depending on their pigment concentrations. The growth and abundance of phytoplankton depends on temperature, light, and nutrient concentrations and is often associated with eutrophication (Vos et al., 2003). Eutrophication is the process of nutrient enrichment in water bodies, particularly from phosphorous and nitrogen (Janssen & Carpenter, 1999). Eutrophication is a natural process, though anthropogenic activity can facilitate it through nutrient enrichment. An increased amount of carbon dioxide, sunlight, and nutrients due to either natural or anthropogenic processes may lead to phytoplankton blooming in aquatic environments. Intense phytoplankton blooms are causing significant and increasing financial losses to aquaculture (Anderson, 2005) resulting in poor aquatic ecosystem conditions. Fish kills can result from anoxia: as algal blooms die off, cell decay leads to oxygen depletion. Human health concerns stem from potential for toxin production by some blue-green algal species. In order to mitigate the impacts, it is very essential to detect, monitor and predict the development and dynamics of phytoplankton biomass in time and space. The conventional ship-based field measurement and analysis techniques are very limited both in spatial and temporal coverage (Ahn & Shanmugam, 2006). Remote sensing (RS) techniques, which utilizes the optical properties of blue-green algal blooms (chlorophyll-a and phycocyanin) can provide data and tools to estimate the phytoplankton biomass with synoptic swath and high temporal frequency.

Chlorophyll-a as a pigment present in most phytoplankton species, is a major indicator of phytoplankton biomass (Doxaran et al., 2006; Moses et al., 2009) commonly monitored from RS to assess the eutrophic status of water bodies. Some phytoplankton groups however contain accessory pigments specific to a smaller group of phytoplankton such as the phycocyanin pigments in cyanobacteria. From hereon the term, Chlorophyll-a (Chl-a) will be used as the measure of phytoplankton biomass.

Predicting the locations and timing of algal blooms using traditional sampling techniques is difficult, if not impossible, due to high variability of conditions in which blooms can form and produce toxins (Schalles et al., 1998). Current methods consist of field sample collection, laboratory analysis, and identification and enumeration of phytoplankton, which can take days to weeks. These methods are neither timely nor cost efficient for drinking water managers since blooms can be as ephemeral as a few days. Because some phytoplankton pigments are optically active and their properties can be measured using spectroscopy, researchers have evaluated the utility of field spectral response patterns for determining concentrations of both chlorophyll a and phycocyanin pigments in lake waters (Mittenzwey et al., 1992; Simis et al., 2005). Researchers have developed models based on variability of spectral response gathered by medium to high resolution spectroradiometers (spectral range approximately 300 to 1100 nm) for sites with differing algal density. Since the optical properties of nuisance algal blooms have been discerned in field reflectance spectra, these remote sensing techniques can be extended to airborne and space borne satellite imaging systems to map chlorophyll-a and phycocyanin concentrations and, therefore, phytoplankton distribution in inland lakes and reservoirs.

Most approaches for remote estimation of phytoplankton biomass are based on the absorption of sunlight by algal pigments in the presence of light scattering by algal cells and non-algal particles. Quantification of Chl-a from RS data in open ocean waters can be fully characterized from the blue and green spectral regions (Dekker., 2003; Gons et al., 2002). These blue-green spectral region however fail at estimating chl-a in strongly absorbing turbid waters (Dall'Olmo & Gitelson, 2005a; Gitelson et al., 2008; Gitelson et al., 2007; Gons, 1999) due the presence of other optically active water constituents. Quantitative estimation of chl-a in turbid productive waters, is carried out by either combinations of reflectance bands (usually band ratios) that exploit the NIR to red spectral region (Dekker et al., 1991) or algorithms that use the Chl-a

fluorescence emission at 685 nm (Dall'Olmo & Gitelson, 2005a; Gower et al., 2004). Many authors have found that the pigment concentration is well correlated to their spectral ratios (Dall'Olmo & Gitelson, 2005a; Dekker et al., 1991; Gons, 1999). The ratio of reflectance near 705 nm to the reflectance near 675 nm is proved useful for retrieval of chl-a concentration [Chl-a] in eutrophic water (Dekker et al., 1991; Gons, 1999). Despite the very low fluorescence signal even in high chl-a concentration areas, the sun induced chlorophyll fluorescence also termed as chlorophyll Fluorescence Line Height "FLH" (Zhao et al., 2008) centred at ~ 685nm may be well correlated to changes in chl-a concentrations and is important indicator of phytoplankton blooming. Dall'Olmo & Gitelson (2005a) have found that the assumptions of constant specific chl-a absorption coefficient and chl-a fluorescence quantum yield upon which such algorithms are based can be significant sources of errors for remote estimation of [Chl-a]. Comparing relations between FLH and [Chl-a] (Gitelson et al., 2007) have found that the variability of fluorescence magnitude in coastal waters can best be attributed to attenuation effects by water constituents, rather than to the differences in fluorescence quantum yield.

Assessment of the contribution of chl-a to remote sensing requires applications of ocean colour sensors with high spatial and temporal resolution. Compared to NASA's wide-swath water colour sensors now in orbit (SeaWiFS and MODIS), the European Space Agency's (ESA) MERIS instrument on board ENVISAT has the advantages of more precise band placement for measurement of chl-a. The fine spatial resolution (300m for all bands) and high radiometric resolution of MERIS data is suitable in determining the signal contributions from dissolved organic matter and detritus materials in the visible (VIS) and near infrared (NIR) spectrum influencing estimation of chl-a. Moreover spectral band configuration of MERIS allows detecting the absorption features caused by phycocyanin (present primarily in cyanobacteria) by their characteristic spectral feature in the MERIS band 6 near 630 nm (Kutser et al., 2006) provided that they are present at detectable concentrations. Cyanobacterial blooms are attracting the attention of environmental agencies and water authorities since they can present a wide range amenity and hazards to human health and animals (Reinart & Kutser, 2006).

The main focus of this study is empirical quantification and mapping of chl-a absorption to study the distribution of phytoplankton biomass in lake Naivasha from the Medium Resolution Imaging Spectrometer "MERIS" and in situ measurements.

1.1. Research Problem

Lake Naivasha is the only inland freshwater lake in Kenya. The outstanding aesthetic scenery and recreational potential makes it well known for boating, water-skiing sports, fishing, game viewing and bird watching. Moreover, the lake is one of biggest source of economic income in Kenya through tourism and the flourishing horticulture and floriculture agricultural activities around the lake. Besides, the lake is also the main source of drinking water supply and hydro-electric power generation (Becht & Harper, 2002) for the town of Nakuru. Apart from the above economic significance, the lake has undergone profound degradation in both quality and quantity (Ballot et al., 2009) which has lead to changes in phytoplankton distribution and decrease in the number of tourists visiting the lake (Mironga, 2006). Economic development and natural ecological and environmental changes around lake Naivasha have resulted in ecosystem damage in the lake. Recent incidents of mass fish die-off are manifestations of change in the lake's water quality.

The water quality degradation which could be attributed to large quantity sediment inflow from Malewa and Gilgil Rivers (Figure 2a), reduced water inflows in low rainfall years or polluting inflows from Naivasha town or from the intensive flower enterprises adjacent to the lake are posing potential threats to the lake's water quality and need detailed investigation and deliberate interventions to ensure it does not deteriorate. In order that the economic values are maintained and the natural ecological environment of the lake is sustained to reduce its hazard on human and animal health, it's of paramount importance that the quality of the water in the lake doesn't deteriorate below acceptable standards.

The need on understanding the water quality status to improve the management practices and the lack of reliable and detailed remote sensing based water quality prediction and monitoring techniques are among the major problems that triggered this study.

1.2. Research Objectives

Understanding the chl-a absorption in time and space in lake Naivasha will help in the monitoring and prediction of the phytoplankton distribution to preserve the natural ecological environment and sustain the economic developments of the lake.

The main objectives of this research are therefore: (1) Investigate the potential of empirical algorithms to estimate chl-a absorption coefficients in lake Naivasha from the in-situ hyperspectral reflectance and absorbance spectra and remote sensing MERIS reflectance spectra. (2) Compare the performance of the three band algorithm by Gitelson (2008), the Synthetic Chlorophyll Index (SCI) empirical algorithm by Shen et al (2010) and the FLH/MCI base line method algorithm by Gower et al. (2004);(2005) to find best model that can accurately estimate and map the variability of phytoplankton distribution in lake Naivasha from MERIS data. (3) Analyze the sensitivity of the proposed model to the spectral locations of the MERIS bands used and validate it using in-situ measurement datasets and address the potential sources of error that limit the utility of the method for this application.

1.3. Research Questions

The main research questions that could be answered in this research are:

1. Are empirical algorithms suitable for estimating the chlorophyll-a absorption coefficient of lake Naivasha from in-situ hyperspectral reflectance, spectrophotometric chl-a absorption and MERIS data?
2. Which of the three empirical algorithms employed best characterizes the optical property of Lake Naivasha?
3. What is the spatial distribution of phytoplankton in Lake Naivasha?

1.4. Research Hypothesis

Hypothesis of interest is in optically turbid inland lakes empirical algorithms band combinations or colour ratios are more accurate at estimating chl-a absorption coefficients from in-situ absorption and reflectance spectra and MERIS data.

1.5. Thesis Outline

This thesis document is generally structured into chapters as: Chapter one will introduce a brief literature review, followed by research problem definition, research objectives, questions and hypothesis. In chapter two the basic thesis concept based on the existing literature will be presented. Chapter three will describe the study area, materials and research methodology used. Chapter four is data analysis method describing the models used in analysing the data to address the research questions and objectives. Chapter five will present the results and discussions of the research. Chapter six will be the conclusions and recommendations of the thesis.

2. LITRATURE REVIEW

2.1. Phytoplankton Bloom Distribution in Lake Naivasha

Several previous studies have demonstrated that the spatial and temporal distribution of the aquatic flora of lake Naivasha has been constrained by two ecosystem-level processes (Harper, 1992). Over the last three decades, the ecology of lake Naiavasha has been subjected to dramatic changes, caused by excessive use of water and catchments area by man (Ballot et al., 2009). Harper (1992) has shown that the natural water level fluctuation and the consequence of herbivory linked to competition between rooted and phytoplankton communities is the factor affecting the ecosystem of the lake. The water-level fluctuations as a consequence of irregular rainfall patterns linked to continental scale climatic events (Harper, 1992) have also influenced the phytoplankton composition and distribution in lake Naivasha.

Hubble & Harper (2002a) used nutrient enrichment studies to investigate the controlling factors for primary production in lake Naivasha and found that nitrogen is more limiting than phosphorus and no persistent vertical stratification of phytoplankton has been observed in the lake due to continuous vertical circulation of the water by wind and convection.

In his investigation of the spatial and temporal patterns of the wet land plant communities in lake Naivasha in relation to the controlling factors (Harper et al., 1995) found that over the past decades the dominant communities include: the emergent swamp dominated by *Cyperus* species; floating raft dominated by the aliens *Salvinia molesta* and *Eichhornia crassipes*; the floating leaved plants represented only by *Nymphaea caerulea*; and the submerged angiosperms consisting of three species of *Potamogetons* - *P. Pectinatus*, *P. schweinfurthii*, *P. octandrus* together with *Najas pectinata*.

Concentration of phytoplankton increased progressively since 1982 as a result of nutrient increase caused by a decline in water level and papyrus swamp clearance for agriculture (Harper, 1992). The dominant phytoplankton community in Lake Naivasha are Cyanobacteria, Chlorophyceae, and Bacillariophyceae, though (Ballot et al., 2009) observed a shift in the dominance of coccoid cyanobacteria towards dominance of Chlorophyceae in the phytoplankton community. Ballot et al (2009) also found that throughout 2002/2003, the Chlorophyceae was the most abundant group and a maximum phytoplankton biomass of 56.6 mg l⁻¹ was recorded during a bloom of *Botryococcus terribilis* in September 2002.

Eutrophication, salinisation and heavy metal contamination in lake Naivasha is mainly controlled by the inflowing rivers enriched in nutrient from catchment areas (Everard & Harper, 2002). Lake Naivasha has one major inflowing river (Malewa) and a number of smaller seasonal rivers (Gilgil, and Karati) (Ballot et al., 2009) as the main sources of water with out any visible surface outlet though an underground outflow through seepage is suggested to keep it fresh (Becht & Harper, 2002).

This high variability of phytoplankton composition and distribution is causing major ecological and social impacts in lake Naivasha through either displacement of indigenous species, habitat alteration, oxygen depletion in the bottom waters and aquaculture (fishes) mortality by poisoning or altering the food-web dynamics. It is therefore crucial to monitor the water quality in time and space based on remote sensing which provides synoptic spatial and temporal coverage.

2.2. Background on Remote Sensing water Quality

Monitoring chl-a distribution over water bodies by conventional (surface) means is hard since they are sporadic in time and isolated in space (Gower et al., 2005; J. Gower et al., 2005)). As a major indicator of phytoplankton biomass, monitoring chl-a distribution over water bodies needs modern technique of remote sensing with a wide-swath and high resolution ocean colour sensors that gives near-daily coverage. The first such measurements were made with the Coastal Zone Colour Scanner (CZCS) which operated between 1978 and 1986 and the pigment concentrations from this sensor were related to the sum of chl-a and phaeophytin-a by an empirical spectral-ratio. With improved spectral and radiometric resolution, the SeaWiFS sensor began producing global maps of chlorophyll-a concentration in September 1997, which

were followed later by MODIS on board the Terra and Aqua platforms and MERIS a multispectral instrument on board ENVISAT for satellite based studies of oceans and continental water bodies. It is therefore important to develop means of obtaining meaningful information from the optical signals recorded by these satellites over water bodies.

Remote sensing allows the collection of information on water quality without having a direct contact with the water body under investigation. Down welling irradiant energy provided by a source such as the sun, is transmitted along a pathway through the atmosphere, reflected off of a target, back into the atmosphere, and then recorded by a sensor. In aquatic systems, the total recorded radiance is a function of path, surface, volumetric, and bottom radiance (Dekker et al., 1991). Path radiance is the result of atmospheric scattering and is classified as noise because it does not contain information on the target water body. Surface radiance describes the top few millimetres of water, the boundary layer between the atmosphere and the water. Volumetric radiance penetrates the boundary layer and provides information about the material suspended in the water column. Bottom radiance passes through the water column and reflects off of bottom sediments. Display of spectral reflectance as a function of wavelength can be used to identify the properties and condition of the target water feature because any optically active water constituents will attenuate or augment the original radiance signal along the spectrum. Since any optically active particle suspended in the water column will affect the irradiance signal, reflectance spectra can be used to estimate productivity, as measured using chl-a concentration. Green algae contain the pigment chl-a which has two absorption maxima at approximately 440 and 675 nm which are commonly exploited in monitoring oceans and inland water bodies respectively. Ocean mapping of chl-a using space borne systems has produced promising results for monitoring productivity. Ocean colour sensors with the necessary spectral bands for detecting phytoplankton pigments, including MODIS, SeaWiFS and MERIS, however, these sensors have a coarse spatial resolution that makes them less favourable for mapping small, inland water bodies. Optically complex inland water bodies, commonly classified as case-II waters are characterized by high concentrations of suspended material, dissolved organic matter, and detritus materials from terrestrial influence. The presence of elevated levels of chl-a and other accessory pigments in inland waters is typically an indicator of high productivity and potentially harmful blue-green algal blooms. Freshwater blue-green algae have an accessory pigment to chl-a, the biloprotein phycocyanin. This accessory pigment allows cyanobacteria to have an additional absorption maximum in the red portion of the spectrum at approximately 620 nm (Gons et al., 1992; Jupp et al., 1994; Kutser et al., 2006; Metsamaa et al., 2006) commonly utilized for mapping phycocyanin pigments in cyanobacteria. Greater variability in the optically active constituents of inland waters also requires increased spectral resolution of sensors.

2.3. Background on Model Types

Since increased algal density causes an increase in both the absorption and scattering coefficients seen in the spectra, many previous investigations have used chl-a absorption as a proxy in measuring productivity in both case I and II water systems. Different optical models are developed for estimating the chl-a content of water bodies from reflectance spectra obtained by remote sensing. Reflectance features for algorithm development are chosen based on the properties of constituent of interest and optical models to be used in estimating water constituent of interest. Morel and Gordon (1980) described three methods for algorithm derivation:

- i. Empirical method – Relationships between spectral reflectance values, $R_{rs}(\lambda)$, and laboratory measured constituent concentrations collected simultaneously are developed using statistical methods.
- ii. Semi-empirical method – Models are based on known spectral features and previously discovered empirical relationships are employed. Measured inherent optical properties (IOP) of the water column are included to derive absorption coefficients for optically active constituents.
- iii. Analytical method – The inherent and apparent optical properties are measured and included in the model as specific absorption and backscatter coefficients. Constituent concentrations are determined

using the reflectance, absorption, and backscatter coefficients. Bio-optical models are constructed based on the biophysical characteristics of a system using radiative transfer equations with the purpose of separating the total radiance into its basic components (Dekker et al., 1991).

Remote sensing reflectance (R_{rs}) at a specific wavelength (λ) is obtained using the ratio of up-welling radiance above the waters surface $L_u(0^+, \lambda)$ to the down-welling irradiance $E_d(0^+, \lambda)$ provided by the sun as measured at a nadir viewing angle as:

$$R_{rs}(\lambda) = \frac{L_u(0^+, \lambda)}{E_d(0^+, \lambda)} \dots\dots\dots \text{Equation 1}$$

Statistically significant relationships between above-water remote sensing reflectance $R_{rs}(0^+, \lambda)$ and constituent concentrations, such as correlation between changes in reflectance with change in constituent concentration as a function of wavelength, are sought and used in algorithm derivation. The following (Gordon et al., 1975) model described the relationship between the inherent optical properties (IOPs), properties of a specific medium independent of a light source, and apparent optical properties (AOPs), properties that are a combination of the IOPs and the light field in which they are measured, is used in development of bio-optical models for homogeneous water bodies with the equation:

$$R_{rs}(0^+, \lambda) = f \left(\frac{b_b(\lambda)}{a(\lambda) + b_b(\lambda)} \right) \dots\dots\dots \text{Equation 2}$$

Where:

$R_{rs}(0^+, \lambda)$ = subsurface reflectance at a specified depth and wavelength

f = experimental factor dependent on the light field (sun angle) and volume scattering function (VSF) (Morel & Gentili, 1991)

$b_b(\lambda)$ = backscatter coefficient (attenuation caused by deflection of energy at certain angles)

$a(\lambda)$ = absorption coefficient (efficiency of a material at absorbing energy)

Subsurface irradiance $R(0^-, \lambda)$ is related to above surface reflectance $R_{rs}(0^+, \lambda)$ by the inclusion of an empirical factor Q , which is the ratio of subsurface down-welling irradiance $E_d(0^-, \lambda)$ to subsurface up-welling irradiance $E_u(0^-, \lambda)$. Specifically the ratio $f:Q$ accounts for the geometry of light exiting the water body on the remote sensing reflectance measured above the water surface. With inclusion of the ratio $f:Q$, $R_{rs}(0^+, \lambda)$ is written as:

$$R_{rs}(0^+, \lambda) \propto \frac{f}{Q} \left(\frac{b_b(\lambda)}{a(\lambda) + b_b(\lambda)} \right) \dots\dots\dots \text{Equation 3}$$

The bio-optical modelling technique requires the inclusion of total absorption, scattering, and backscatter coefficients. In the radiative transfer model for case II waters, total absorption and backscattering coefficients for three optically active constituents of natural water bodies are:

$$a(\lambda) = a_w(\lambda) + a_{phy}(\lambda) + a_{NAP}(\lambda) + a_{CDOM}(\lambda) \dots\dots\dots \text{Equation 4}$$

$$bb(\lambda) = bb_w(\lambda) + bb_{phy}(\lambda) + bb_{NAP}(\lambda) + bb_{CDOM}(\lambda) \dots\dots\dots \text{Equation 5}$$

Where:

$a_w(\lambda)$, $bb_w(\lambda)$ = absorption and backscatter coefficients for pure water at wavelength (λ) (Pope & Fry, 1997)

$a_{phy}(\lambda)$, $bb_{phy}(\lambda)$ = absorption and backscatter coefficients for phytoplankton at wavelength (λ)

$a_{NAP}(\lambda)$, $bb_{NAP}(\lambda)$ = absorption and backscatter coefficients for none algal particles at wavelength (λ)

$a_{CDOM}(\lambda)$, $bb_{CDOM}(\lambda)$ = absorption and backscattering coefficient for coloured dissolved organic matter at wavelength (λ)

According to Beer’s Law, it is assumed that absorption and scattering properties of a water body are a linear function of the concentration of its constituents. The absorption coefficient for the optically active constituent of interest divided by the specific absorption coefficient, $a^*(\lambda)$, absorption per unit path length and mass concentration, can yield pigment concentration (Gons, 1999):

This research has compared the following three empirical algorithms to assess a best fit model for the prediction of phytoplankton absorption coefficients in Lake Naivasha using MERIS data (Table 1).

The three band algorithm by Gitelson et al (2008); Synthetic Chlorophyll Index(SCI) by Shen et.al .(2010) and the Fluorescence Line Height (FLH) baseline method by Gower et al. (2004) and in a similar technique as the FLH; the Maximum Chlorophyll Index (MCI) by Gower et al. (2005) were analyzed against the in-situ spectrophotometric absorption, Trios reflectance and MERIS derived reflectance using least squared regression techniques.

Chlorophyll a empirical algorithms	publication by
$[R_{rs}^{-1}(\lambda_1) - R_{rs}^{-1}(\lambda_2)] \times R_{rs}(\lambda_3) \propto a_{chl a}(\lambda_1)$	(Gitelson et al., 2008)
$SCI = H_{chl} - H_{\Delta}$ $H_{chl} = \left[R_{rs}(\lambda_1) + \frac{\lambda_2 - \lambda_1}{\lambda_3 - \lambda_1} (R_{rs}(\lambda_3) - R_{rs}(\lambda_1)) \right] - R_{rs}(\lambda_2)$ $H_{\Delta} = R_{rs}(\lambda_2) - \left[R_{rs}(\lambda_4) + \frac{\lambda_2 - \lambda_4}{\lambda_3 - \lambda_4} (R_{rs}(\lambda_3) - R_{rs}(\lambda_4)) \right]$(Shen et al., 2010)
$FLH = Rrs(B_8) - Rrs(B_9) - \frac{[(Rrs(B_7) - Rrs(B_9)) \times (B_9 - B_8)]}{[B_9 - B_7]}$ $MCI = Rrs(B_9) - Rrs(B_{10}) - \frac{[(Rrs(B_8) - Rrs(B_{10})) \times (B_{10} - B_9)]}{[B_{10} - B_8]}$(Gower et al., 2005; Gower et al., 2004)

Table 1 List of empirical algorithms employed to derive chl-a from lake Naivasha.

3. STUDY AREA MATERIALS AND METHODOLOGY

3.1. Study Area Description

Lake Naivasha is fresh water lake situated in the eastern Rift Valley of Kenya at a latitude of 0o5'South and 36o20'East longitude. It is an enclosed basin located at about 80kms SE of the capital Nairobi and has an altitude of approximately 1890m. Rainfall is bimodal with peaks in April and October (Hubble & Harper, 2002b), but shows inter annual irregularity and annual evapotranspiration exceeds rainfall (Harper et al., 1990). The average annual rainfall is around 680 mm in two rainy seasons which is normally exceeded by the annual evapotranspiration that results in instability the lake size. Though fluctuation in lake level (Harper et al., 1995) with in flows is evident, lake Naivasha is the second largest fresh water lake in Kenya with an average surface area of 160 km² (~16 X 10 km) and is accessible by all weather roads within the area.

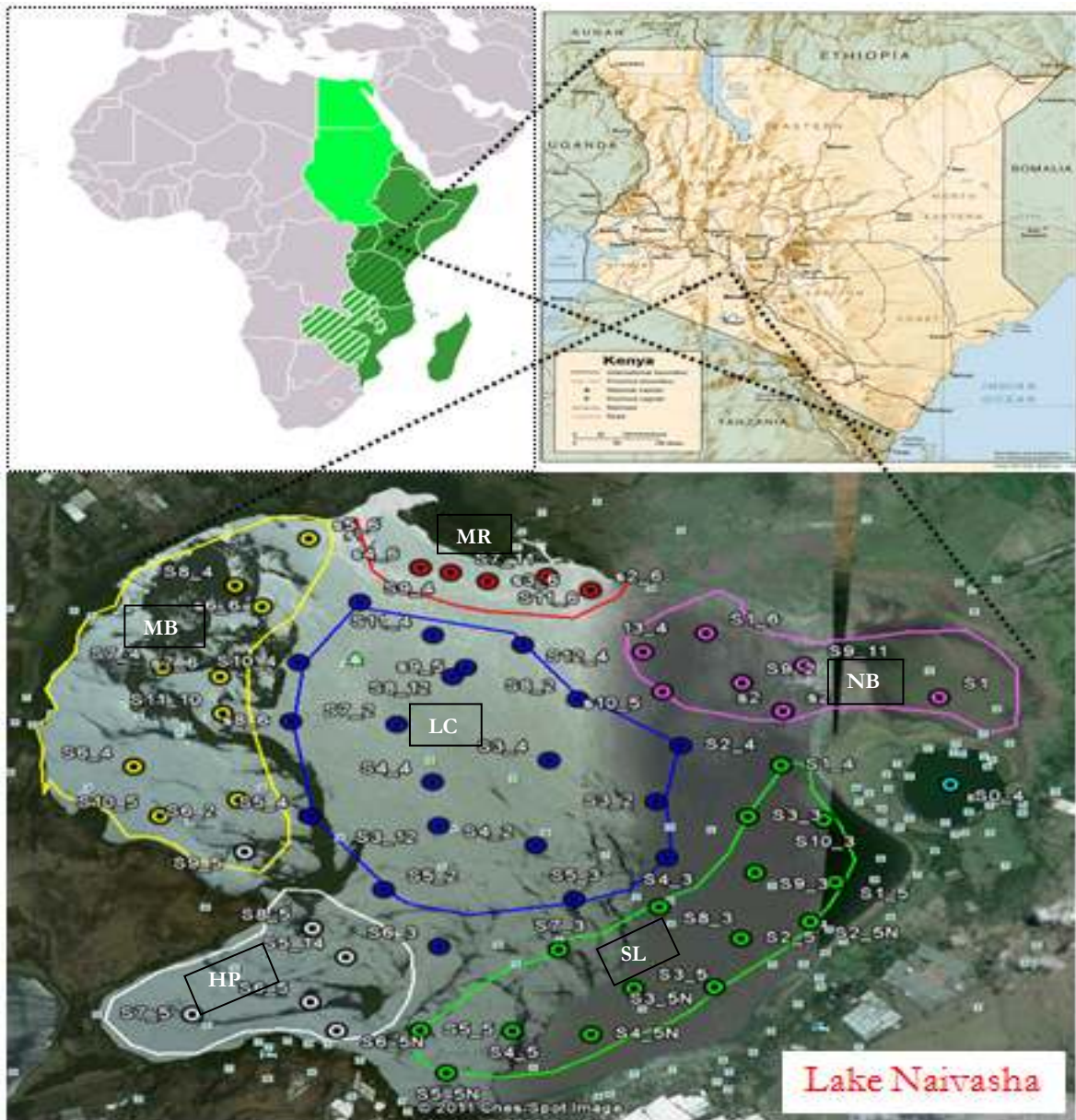


Figure 1. Location map and field measurement points distribution.

Study area in sub-regions (bottom) the Crescent Island lagoon indicated (S0_4) in the east, the lake centre(LC) stations indicated in (Blue), the Safariland Bay (SL)stations indicated (Green) in the south and southeast part of the lake, the Hippo-pint stations indicated in (white) southwest of the lake, the Mennel's bay (Yellow) in the west and northwest, the Malewa river mouth (MR) indicated (Red) in the north, the Naivasha town Bay (NB) indicated in (Pink) in the northeast part of the lake. Location naming adopted from (Harper et al., 1995).

Lake Naivasha, is mainly fed by three inflowing rivers (Malewa, Gilgil and Karati) with out any visible surface outlet though an underground outflows is suggested (Becht & Harper, 2002) which keeps the lake fresh. River Malewa which begins in the western slopes of the Aberdares ranges in central Kenya is the dominant river flowing south through highly manipulated small and large-scale farms before making its entry into the lake on the northern shores. This rivers are generally believed to play an important role in the quality of the lake by carrying large amount of sediments and other nutrients which influences its area, limnology and hence its productivity (Becht & Harper, 2002).

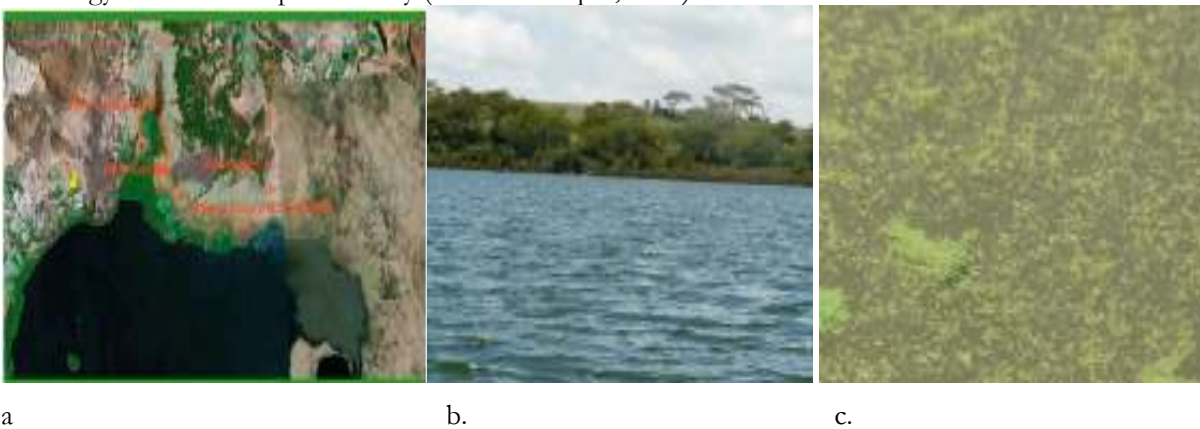


Figure 2. Malewa and Gilgil flood plains, Crescent Island lagoon and Main lake water condition.

(a) Landsat image of northern shore of lake Naivasha indicating the Malewa and Gilgil river flood plains. Sediment inflows in lake Naivasha are believed to be from the catchments of these rivers. (b and c) indicate particulate matter content difference in Crescent Island and main lake Naivasha. Photo (b) taken on a pier at Crescent Island lagoon and photo (c) taken on a pier at the center of the main lake on the 20th of September 2010.

3.2. Sampling and Radiometric Measurement Distribution

Data were collected from the main lake Naivasha and the Crescent island lagoon during one cruise in 2010 (from September 17 through October 03). A total of about 170 stations were sampled and measured for optical signals both from the Crescent Island and the main lake. Measurements of water constituents from the main lake were grouped into sub-regions based on their geographic locations and possible range of optical variations (Figure 1) for the purpose spatial analysis. 14 stations were collected from the Mennel's Bay located north of the Hippo-point; 8-stations were collected from the Malewa river mouth or the North Swamp; 19- Stations were collected from the Safari-land Bay close to the flower farm; 5-stations were collected from the Naivasha Town Bay. Additional radiometric measurements were also collected from some of the above regions during the satellite overpass time for the purpose of obtaining more match-up date measurements (Table 5)The sampling locations were chosen to cover as wide range of optical conditions as possible. The sampled water body was relatively shallow (average depth between 3-6 m), with relatively small surface areas (160 m²). A total of about 137 contemporaneous absorption spectra were measured from the stations measured for radiometric signals.

3.3. Description of Materials Used

To retrieve the phytoplankton absorption coefficient of Lake Naivasha and assess the accuracy and performance of the algorithms used in predicting chl-a absorption, two independent datasets; an in-situ radiometric and laboratory datasets and MERIS data containing spectral optical properties of the water column were used.

3.3.1. In-Situ Datasets

The in-situ datasets were collected on one cruise in Lake Naivasha during the field work carried out from the 17th of September to the 3rd of October 2010. This dataset was divided into calibration and validation datasets for algorithm calibration and validation. Radiometric measurements with reliable contemporaneous analytical data were selected and used in the model calibration and validation purposes. The second dataset contains five MERIS match up date data taken on September 2010 during our field period. Two of these satellite images are partial affected by cloud cover while the rest three images are free of cloud (Table 3). Due to frequent cloud development in the area especially during afternoon periods, all in-situ radiometric measurements were collected before noon from 09:00 to 12:00 a.m. This measurement time agree with the satellite overpass time over lake Naivasha (Table 4) and concurrently water samples were collected from each station and immediately analyzed in the lab for phytoplankton absorption coefficients. A total of about 172 stations were measured for above and below water radiometric signals and contemporaneous 137 stations were sampled for water and analyzed for phytoplankton pigment absorption using a spectrophotometer. Radiometric measurement from three stations complexly erratic and only 169 stations were processed. The first day spectrophotometric absorption measurements were also highly affected by measurement errors and spectra from only 127 stations were processed (Table 5). Each measurement station was geo-located using a GARMIN GPS devise for mapping purposes. The radiometric measurements were carried out from a ship using radiance and irradiance sensors mounted on a hand held 2m black metal bar.

Statistical parameter	Phytoplankton Absorption Coefficients (m^{-1})				Number of Samples	a_{CDOM} (440nm) m^{-1}	a_{NAP} (440) m^{-1}	SPM mg/m^{-3}	Sechi Disc Depth(m)
	440nm	560nm	620nm	665nm					
Mean	2.28	0.16	0.09	0.15	137	2.68	5.55	33.95	0.39
Max	3.28	0.27	0.18	0.30		3.92	14.93	101.25	0.51
Min	1.06	0.024	3×10^{-4}	0.01		0.92	0.00	1.00	0.27
Stdev	0.48	0.048	0.04	0.05		0.64	2.94	16.87	0.10

Table 2. Statistical summary of averaged in-situ measurements

The above table shows the in-situ absorption coefficients of phytoplankton (a_{phy}) at the specified wavelengths, number of samples used, absorptions by CDOM, NAP and SPM concentrations for the aggregate dataset in lake Naivasha and sechi-disc depth values in the main lake Naivasha.

3.3.2. Remote sensing Datasets

For the present study, a multispectral instrument the MEdium Resolution Imaging Spectrometer (MERIS) on board the ENVIronmental SATellite (ENVISAT) platform was used. MERIS is a push broom imaging spectrometer operating in the visible and near-infrared (VNIR) spectral range from 400 to 900 nm. It has a wide field of view (FOV) of 68.5° around nadir, which leads to a swath width of 1150 km at an altitude of 800 km. Ground sampling distance of MERIS is about 300 m for full spatial resolution (FR) data and about 1.2 km for reduced spatial resolution (RR) data. One of the major the advantages of MERIS is its band placement and sensitivity to the most important optically-active water constituents. For example, retrieval of yellow substances (coloured dissolved organic matter and detritus) (412.5 nm), chlorophyll

absorption (442.5, 490, and 665 nm), turbidity (510, 620 nm), red tides (510 nm), and chlorophyll fluorescence (665, 681, and 709 nm) are applications used with MERIS.

Due to the frequent cloud cover, it was difficult to obtain a series of cloud free images of the area over a longer period of time. Available cloud free MERIS Level 1b images of the study area were downloaded from the ESA archive on request (Table 3). This data archive hosted by the European Space Agency is readily accessible and available on request on the internet. The MERIS scenes were downloaded using the EOLISA Viewer tool available at <http://earth.esa.int/EOLi/EOLi.html>.

Level-1b MERIS (FR) data covering lake Naivasha were ordered from the European space Agency after the necessary visualization using the Earth Link (EOLI) viewer from the ESA web site for quality prior to ordering. Five full resolution (FR) MERIS scenes of lake Naivasha acquired on the field measurement period September 17th, 20th, 23rd, 26th and 29th of 2010 (Table 4) were downloaded from the ESA archive and due to in-situ data validity and cloud coverage the 17th and 29th images were excluded from match-up date validation processes.

These TOA radiances were processed and converted to remote sensing reflectance (R_{rs}) to be used as inputs in to the models to retrieve the absorption coefficients of phytoplankton. This reflectance signal however contain significant atmospheric noises due to the absorption and scattering of the light by the atmospheric gasses and dust particles, images were corrected for this noise before any further analysis is carrying out.

Satellite data

No.	Date acquired	Platform	Sensor	Resolution	Cloud cover
1.	September 20 th /2010	ENVISAT	MERIS	FR	0%
1.	September 23 rd /2010	ENVISAT	MERIS	FR	0%
1.	September 26 th /2010	ENVISAT	MERIS	FR	0%

Table 3. Summary of earth observation data used in the study.

General characteristics of MERIS FR images over lake Naivasha; over-pass time, viewing and illumination angles, and weather conditions as observed during field work are:

Date	17/09/10	20/09/10	23/09/10	26/09/10	29/09/10
Satellite over pass					
Time (UTC)	07:18:54	07:24:34	07:30:15	07:35:53	07:41:32
Sun zenith	32.70 deg	31.00 deg	29.28 deg	27.56 deg	25.90 deg
Sun azimuth	84.50 deg	86.62 deg	88.79 deg	91.19 deg	93.94 deg
View zenith	31.16 deg	20.95 deg	08.96 deg	04.10 deg	16.72 deg
View azimuth	102.53 deg	102.49 deg	102.47 deg	282.45 deg	105.3 deg

Weather conditions: No visible clouds were over on the images of 20th, 23rd, and 26th but the image on the 29th September 2010 has partially cover and was not used for mapping.

Wind, wave height a few cm

Local time is UTC+3

Table 4. Characteristics of MERIS data in lake Naivasha.

3.4. Methodology

A field campaign was carried out from September 17th to October 3rd of 2010 on lake Naivasha. Ground truth water samples were collected simultaneously with field spectral measurements for analytical investigations (Table 2). This study was designed to establish relationships between field spectra and algal pigment absorption which is directly related to chl-a concentration while also assessing the influence of additional water quality parameters on the robustness of these relationships.

Detailed descriptions of the analytical methods and data processing used for the treatment of the measured variables are presented below. To study the spatial characteristics of the lake, the measured spectra were analyzed in sub-regions based on the prevailing optical variations, geographic locations, natural and anthropogenic influences as:

For the purpose of spatial investigations the lake was analysed by dividing the main lake measurement stations into sub regions as: Hippo Point (HP) stations, Malewa River mouth (MR) stations close to the main inflow, the Safari land Bay (SL) close to the flower farm, the Mennell's Bay (MN), the Naivasha town Bay, and Crescent Island lagoon (Cr) a partially separated crater within the main lake (Figure 1). Sub-region naming is adopted from (Harper et al., 1995). The following flow chart is the general methodology followed in this research:

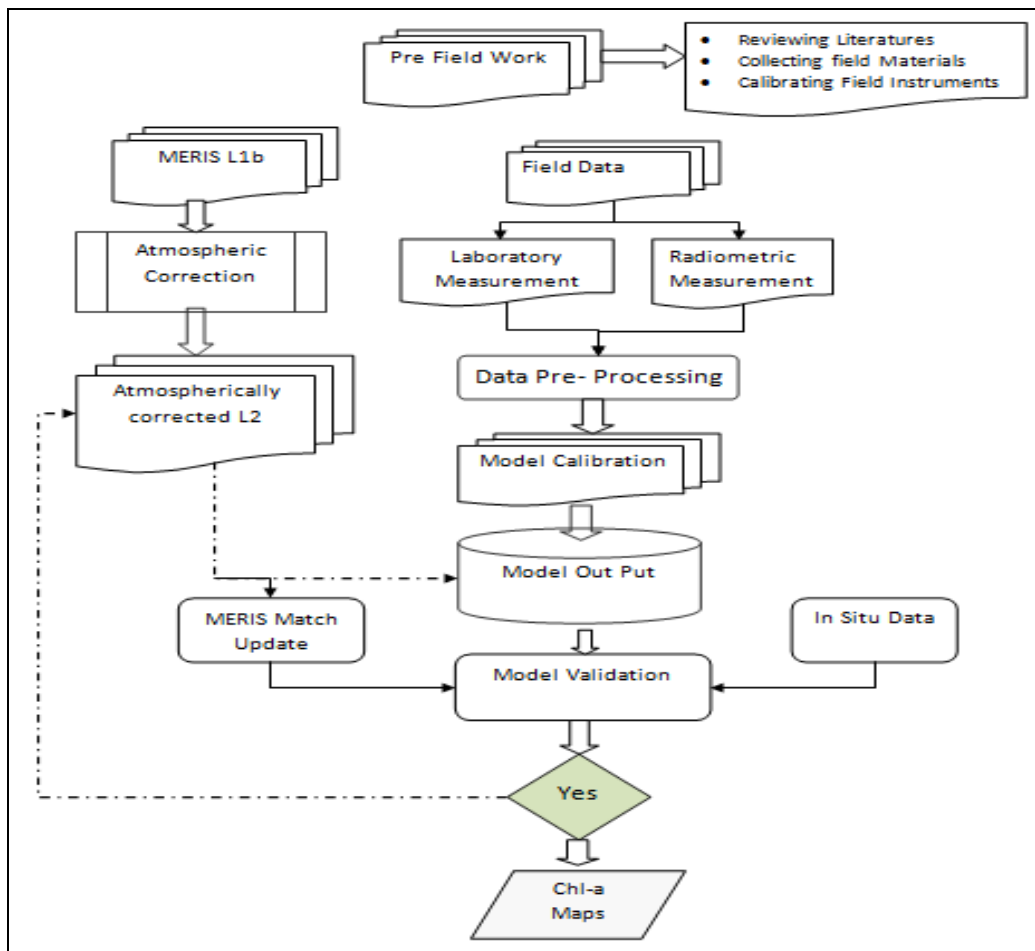


Figure 3. Schematic representation of the general methodology.

The above flow chart shows the general research methodology followed. Dashed lines indicate steps on the application of the method to remote sensing data.

3.4.1. Data Collection

A field campaign was carried out from September 17th through October 3rd 2010. A 9 to 13 measurement stations per day were sampled and measured for radiometric signals covering the lake in every fourth day. All the measurements and sampling tasks were scheduled out before noon to take advantage of the satellite overpass time 10:18 to 10:41a.m (Table 4) and also to avoid the interferences in illumination conditions due to the frequent cloud appearances in the afternoon. Water samples were collected at 5-10 cm depth below the water surface to the extent possible, with primary limiting factors being to sample at the same level through out the measurement period. Although most of the measurements were carried out under clear sky conditions, some measurements were taken under diverse range of illumination and weather conditions whereby cloud and wind developments could have interfered and affected the readings.

The measured IOPs and optical measurements used as an input for the empirical algorithm were from 90 sampling sites. Measurements from 47 stations were excluded from further analysis due to several errors introduced in the chl-a extraction and $R_{rs}(\lambda)$ spectra measurements. The possible source of errors could be instrument accuracy, errors in pigment extraction, movement of the boat while taking optical measurement, cloud spot, aquatic suspended vegetations, measurement errors, sun glint, water surface roughness, shallow depth and foam.

Measurement Type	Samples Collected	Samples Analyzed	Samples Processed	Samples Retained	Samples Used
Radiometric Measurement	172	172	169	169	90
Spectrophotometric	137	137	127	90	90

Table 5. Samples Collected, processed and retained

3.4.1.1. Laboratory Measurements

Measurement of chl-a requires its extraction from planktonic cells, which involves filtering the water as the first step, then extracting the filter with an appropriate solvent. Once the extracts are obtained, chl-a is measured using spectrophotometric or fluorometric procedures. In this research water samples were collected few (5 to 10) centimetres below the surface using sample bottles properly rapped with aluminium foil to minimize chl-a degradation upon interaction with direct sunlight and temperature. Depending on the amount of suspended particulate matter and filtration capacity of the filters used, 100 to 350 ml of water from samples to be analysed for chl-a absorption were filtered through 0.7 μm pore size Whatman GF/F filter with an appropriate vacuum pressure according to (IOCCG Ocean optics Protocol Revision 5 Volume V). The chlorophyll pigment retained on the filters was extracted through grinding in 90% acetone in a glass homogeniser vessel with a pestle. To remove particles of diameters between 0.22 μm and 0.7 μm the extract was allowed to be filtered again through a 0.22 μm Millipore cellulose acetate membrane filter (Aminot & Rey, 2000) before measuring its absorbance in a spectrophotometer. There are several techniques of pigment extraction for spectrophotometric absorbance measurements. This method uses 90% acetone as the extraction solvent because of its efficiency for most types of algae (Binding et al., 2004). In Chl-a extraction using acetone solution, grinding of the filters is recommended instead of sonicating or soaking over night (Aminot & Rey, 2000). After extraction samples were centrifuged for about 10 minutes to avoid the transfer of any suspended particles from the filtrate to the optical cuvette. Centrifuged extracts were then carefully transferred to a 1cm length optical Cuvette to measure chl-a absorbance (optical density) at selected wave lengths. The pestle was then carefully rinsed using 5 ml of the buffer solution before each next sample is put on to it for extraction.

3.4.1.2. Radiometric Measurements

Radiometric (radiance and irradiance) measurements, above and below water surface were carried out from 17th of September to 3rd of October 2010 using hand held spectro-radiometers mounted on 2m black metal bar from a boat. A Trios RAMSESARC radiance sensor (7° field of view, 318–951 nm), and a Trios RAMSES-ACC-VIS irradiance sensors were used to measure the radiance and irradiance signals in the lake according to the NASA protocol of optical measurements. The radiance sensor was pointed downward to measure the above water up welling radiance $L_u(\lambda)$ at nadir. The tip of the radiance sensor was kept just above the water surface on the sunny side of the boat with the 2m black pole. Though most measurements were carried out on the absence of waves, some measurements taken during windy conditions were affected by waves of moderate sizes. Some measurements taken towards noon were also impacted by specular reflection off the surface of the water. The down-welling irradiance $E_d(\lambda)$ was measured simultaneously as the radiance by the irradiance sensor mounted on the same metal bar pointing upwards to collect the total incoming radiation from the sun. The variations in illumination conditions between measurements were considered negligible during the short time taken to collect one measurement (~ 10 seconds) and the data recorded by the irradiance sensor is considered representative of the overall down-welling irradiance. However, this second sensor failed after some days of measurement, and the down-welling irradiance measurement was continued indirectly by the radiance sensor and a Spectralon reference panel. The radiance signals recorded from the white reflectance panel were then converted to irradiance by multiplying by (π) and dividing by reflectance efficiency of the reflectance panel 0.99 to correct the bidirectional reflectance effect (Doxaran et al., 2006). The radiance and irradiance signals from both sensors were pre-processed and quality checked before computing the water leaving reflectance which was used in retrieving water quality parameter of interest. Radiometric data concurrent to MERIS overpass times was used for match up date validation purposes of the model.

3.4.2. Data Processing

3.4.2.1. Phytoplankton Absorption Coefficient

Phytoplankton absorption is often inferred from measurements on cells retained on glass fiber filters or from measurements in suspension provided that the concentration of the phytoplankton in the water column allows such a determination. The measurement of algal biomass is important in aquatic studies, which is most commonly estimated from determinations of chl-a. The most frequently used methods of chl-a determination from freshwater algae involve spectrophotometric analysis at selected wavelengths of the pigments in suspension on different solvents. The optical density (absorbance) measurements need to be converted to absorption coefficient prior to its implementation on the empirical algorithms for calibration and validation purposes. The measured spectral absorbance was converted to the spectral absorption coefficient following (Binding et al., 2004; Mitchell et al., 2002) which is one of the inherent optical properties that influence the reflectance of aquatic systems.

The phytoplankton absorption coefficient $a_{phy}(\lambda)$ in units of m^{-1} was parameterized from the absorbance as:

$$a_{phy}(\lambda) = \frac{2.303A_f}{V_f} [[OD_{sl}(\lambda) - OD_{bl}(\lambda)] - OD_{null}] \dots\dots\dots \text{Equation 6}$$

Where: $OD_{sl}(\lambda)$ is the measured optical density of the sample filtered, $OD_{bl}(\lambda)$ is the optical density of a blank solution, and OD_{null} is a null wavelength residual correction from the infrared where particle absorption is minimal. For spectrophotometers with automatic base line correction and a flat reference filter base line there is no need to subtract for $OD_{bl}(\lambda)$ (Pope & Fry, 1997). In order to conform to the convention used throughout the ocean optics protocols, it is necessary to convert the OD measurements to the base-e representation of absorbance, i.e. to multiply by 2.303.

To correct for residual offsets in the sample filtrate relative to the reference, and for scattering losses due to particle loading, it is assumed that a null absorption wavelength in the infrared can be characterized by

the 750 nm null absorption wavelength, though recent reports indicate that this wavelength is too short for some waters (Pope & Fry, 1997).

The $OD_{bl}(\lambda)$ was dropped for the automatic baseline correction DR2000 spectrophotometer used and (Eqn.6) was rewritten as:

$$a_{phy}(\lambda) = \frac{2.303A_f}{V_f} [OD_{st}(\lambda) - OD_{null}] \dots\dots\dots \text{Equation 7}$$

Where:

The OD_{null} is the optical density for the null wavelength absorption (750nm, in this case)

A_f is the surface area in m^2 of the filter from which sample is extracted.

V_f is volume of water filtered in millilitre.

In this research the whattman GF/F used was 55 mm in diameter with a sample extraction diameter of 35 mm. The sample extraction surface area as computed from the measured filter diameter containing the pigment of interest was approximately equal to $0.000962 m^2$.

3.4.2.2. Radiometric processing

Field radiometric (radiance and irradiance) measurements were carefully analysed visually for noises prior to any processing. Stations with value above and below 95% confidence interval were considered as measurements affected by either specular surface reflection or cloud and were excluded from analysis. The above water up-welling radiance was then normalised to the down-welling irradiance above water to derive the remote sensing reflectance (Eqn.1) to be used in the analysis and validation of the remote sensing data after atmospheric correction.

$$R_{rs}(\lambda) = \frac{L_u(0^+, \lambda) - F \times L_{sky}(\lambda)}{E_d(0^+, \lambda)} \dots\dots\dots \text{Equation 8}$$

Where:

F is surface Fresnel reflectance (air-water interface specular reflection coefficient for radiance).

L_{sky} is sky radiance (radiance contributed into the sensor from the surrounding). Considering low wind speed (less than 2m/sec) and calm water surface roughness during measurement period, the factor ($F \times L_{sky}$) was negligible and hence, up welling water radiance and down welling irradiance was used to derive remote sensing reflectance using the relation in (Eqn.1):

For some measurements of down welling irradiance were carried out indirectly using the radiance sensor and a spectralon reflector ($L_R(\lambda)$), after RAMSES-ACC-VIS sensor was failed to transfer data to the logger, the down-welling irradiance was derived through the following relation (Lee et al., 2007):

$$E_d(0^+, \lambda) = \frac{L_R(\lambda) \times \pi}{R_R} \dots\dots\dots \text{Equation 9}$$

$$R_{rs}(\lambda) = \frac{(L_u(0^+, \lambda) - F \times L_{sky}(\lambda)) \times R_R}{\pi \times L_R(\lambda)} \dots\dots\dots \text{Equation 10}$$

Where:

R_R is the reflectance of the diffuse reflector (0.99) (Doxaran et al., 2006). Considering the negligible water surface reflectance due to the calmness of the lake water surface, $R_{rs}(\lambda)$ can be computed as follows:

$$R_{rs}(\lambda) = \frac{(L_u(0^+, \lambda)) \times 0.99}{\pi \times L_R(\lambda)} \dots\dots\dots \text{Equation 11}$$

3.4.2.3. Atmospheric Correction

The first step in ocean colour remote sensing is the derivation of the water-leaving radiance $L_w(\lambda)$ at a wavelength λ through atmospheric correction (Gordon et al., 1983). This process converts the top of atmosphere (TOA) radiance into water leaving reflectance by normalization of illumination conditions and removal of atmospheric effects (Guanter et al., 2010). The accuracy of the information obtained from ocean colour sensors hence largely depends on the accuracy of the atmospheric correction model used to estimate the atmospheric contribution on the radiance leaving the water surface. Atmospheric path signal due to air molecules, aerosols, and the air-sea interface accounts to more than 90% of the total signal recorded at the top of the atmosphere (TOA) (Ahn & Shanmugam, 2006; Siegel et al., 2000). These signals are noises to the radiance leaving the water column and should be corrected with a correct atmospheric correction scheme.

Unlike the open ocean (clear) waters, the water leaving radiance in NIR spectral region in turbid inland lakes can not be assumed zero (Moore et al., 1999). The non-negligible value of water leaving reflectance at the NIR has been accounted by many authors Salama & Shen (2010), Siegel et al.(2000) and Vermote et al.(2002). Salama & Shen, (2010) have recently estimated successfully the backscattering and aerosol reflectance in the NIR simultaneously which will improve the accuracy of the retrieved pigment concentration. There are different atmospheric correction methods developed for estimating the aerosol concentration, a major component in the atmosphere influencing the estimation of constituent of interest. In this research, ignoring direct sun glint as most of the measurements were collected before noon and assuming that the sea surface is flat for low wind speed conditions, the total radiance $L_t(\theta_0, \theta, \Phi_0, \Phi)$ recorded at the sensor level where θ_0, θ , are the sun and sensor zenith angles respectively and the Φ_0, Φ are the relative azimuth angle is combination of different constituents. Dropping the viewing geometry for brevity, this term can be divided into its components as:

$$L_t(\lambda) = L_r(\lambda) + L_a(\lambda) + T_v[L_{sfc}(\lambda) + L_w(\lambda)] \dots \dots \dots \text{Equation 12}$$

Where: L_r is radiance resulting from scattering by air molecules(Raleigh scattering) in the absence of aerosols, L_a is the contribution from aerosol scattering in the absence of air, L_{sfc} is the contribution from the surface, T_v is the viewing diffuse transmittance of the atmosphere and L_w is the desired water leaving radiance.

Converting the radiance to reflectance as:

$$Rrs_t(\lambda) = \frac{\pi L_t(\lambda)}{E_0(\lambda) \cos(\theta_0)} \dots \dots \dots \text{Equation 13}$$

Where: E_0 is the extraterrestrial solar irradiance and θ_0 is the solar zenith angle.

Similarly the total reflectance $Rrs_t(\lambda)$ at the sensor can be written as:

$$Rrs_t(\lambda) = T_g(\lambda)[T_v(\lambda)Rrs_{sfc}(\lambda) + Rrs_{path}(\lambda) + T_v(\lambda)Rrs_w(\lambda)] \dots \dots \dots \text{Equation 14}$$

Where: $T_g(\lambda)$ and $T_v(\lambda)$ are the gaseous and viewing diffuse -transmittance from the ocean to the sensor respectively. The subscripts in the equation represent the contribution from atmospheric path *path*, surface *sfc*, and water *w*.

$Rrs(\lambda)$, the portion of the light that enters the water body, absorbed and scattered back to the sensor by the water constituents and the water column is the quantity required in ocean colour remote sensing that can be related to the physical property of the water body.

$Rrs_{sfc}(\lambda)$, the contribution from the surface of the water body is considered very small (at low wind speeds) conditions and hence is dropped.

Due to the presence of the atmosphere, a considerable amount of the incident radiation $Rrs_{path}(\lambda)$, is attenuated or scattered back to the sensor without reaching the water body which is undesired signal recorded together with the water leaving reflectance by the sensor.

(Eqn.14) can be farther simplified with above assumptions as:

$$Rrs_t(\lambda) = T_g(\lambda)[Rrs_{path}(\lambda) + T_v(\lambda)Rrs_w(\lambda)] \dots\dots\dots\text{Equation 15}$$

Where: T_g and T_v are the gaseous and viewing diffuse transmittance, Rrs_{path} and Rrs_w are the reflectance contributions from the atmosphere and water respectively.

The water leaving reflectance (WLR) Rrs_w can be extracted from total received reflectance at the sensor (Eqn.15) as:

$$Rrs_w(\lambda) = \frac{Rrs_t(\lambda) - Rrs_{path}(\lambda)}{T_v(\lambda)} \dots\dots\dots\text{Equation 16}$$

The $Rrs_{path}(\lambda)$ and $T_v(\lambda)$ values for the MERIS images where concurrent in-situ measurements were available were estimated using micro-soft excel solver program at the minimum RMSE values between the in-situ measured water leaving reflectance and MERIS (Table 6). Comparison of the averaged corrected MERIS reflectance and the contemporaneous averaged in-situ reflectance measurement for the 20th, 23rd and 26th of September 2010 showed good correlation resulting in r^2 and RMSE values of 0.885, 0.988, 0.964 and 0.009236, 0.002583, 0.007 respectively in the NIR spectral region (Figure 4).

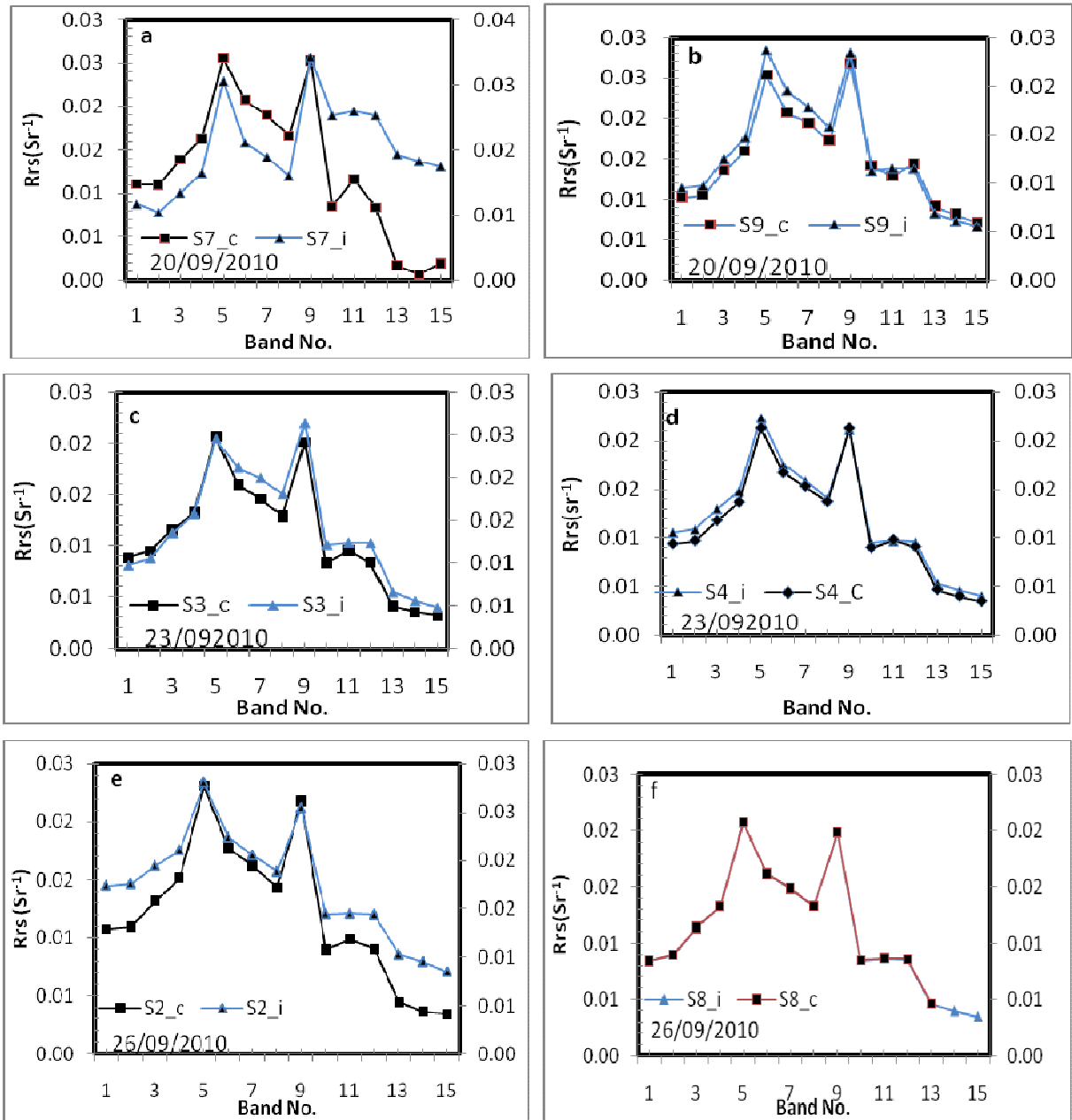


Figure 4. Comparison between in-situ and MERIS derived reflectance spectra.

The above plots show worst and best results of the correction method comparing in-situ remote sensing reflectance and MERIS derived reflectance spectra on the 20th, 23rd, and 26th of September 2010 taken in different stations. The comparison was done excluding stations 0 and 1 of each date where signal was constantly affected by the adjacent land pixels.

4. DATA ANALYSIS METHODS

4.1. Spectral Analysis

The relationship between field spectral responses and analytically measured phytoplankton pigment absorption coefficients, a_{phy} was determined by the application and optimization of the previously developed algorithms (Table 1). Least squared regression technique was applied to relate the in situ chl-a absorption coefficient and the model result and determine the best fitting coefficient for the models. The strength of the relationship between the empirical algorithm and analytically measured pigment absorption coefficients were evaluated using the r^2 and RMSE from the least-squares regression analysis. Coefficients derived using regression analysis were applied to the remote sensing dataset MERIS to retrieve and map phytoplankton absorption coefficients for lake Naivasha. A model that proved a strong relationship between model index values obtained from each algorithm against and analytically measured phytoplankton pigment absorption coefficient was used to map the phytoplankton absorption coefficient of the lake for visualisation.

4.2. Summary of Spectral Reflectance Features Observed

Three optically active components affect the features found in the spectral reflectance curve of freshwater: phytoplankton pigments, particulate matter, and yellow substances. Several previous researches have identified some of the sources of the features found in the curve (Figure 5) of field reflectance spectra from lake Naivasha. The absorption feature found at approximately 440 nm (Figure 5a), is attributed to absorption by chl-a (Gitelson et al., 1999). This feature is used in ocean colour models to estimate the chl-a content in deep ocean waters although this spectral region is not recommended to inland waters due to the presence of dissolved organic matter and suspended sediment significantly affecting the signal. An additional absorption feature within the range of 450 and 525 nm (Figure 5b) is caused by presence of carotenoids (Gitelson et al., 1999; Gitelson et al., 1995; Rowan, 1989; Yacobi et al., 1995). Carotenoids are a class of yellow to red pigments that include carotenes and xanthophylls. The spectral range of 550 to 600 nm (Figure 5c) contains the green peak, mostly due to minimal absorption by phytoplankton pigments and, thus, maximum scattering by algal cells (Dekker et al., 1991; Gitelson, 1992; Gitelson et al., 1995). It has been suggested that a shift in this peak toward longer wavelengths is a result of absorption of the shorter wavelengths by carotenoids, indicating an increased carotenoid concentration. A shift in the green peak toward shorter wavelengths (540 nm) is caused by absorption of the longer wavelengths by phycocyanin, a pigment found in cyanobacteria, indicating an increase in phycocyanin concentration (Gitelson et al., 1999; Schalles et al., 1998). The subsequent trough, within the range of 620 and 630 nm (Figure 5d), is the result of absorption by phycocyanin (Schalles et al., 1998). The minor reflectance peak at approximately 650 nm (Figure 5e) is attributed to backscattering from dissolved organic matter (Gitelson, 1992). This feature is also known to be affected by phycocyanin concentration because it is the location of the phycocyanin fluorescence emission maximum (Ahn et al., 1992). The trough feature at approximately 675 nm is the chlorophyll a absorption maximum (Figure 5f) (Han & Rundquist, 1997). The reflectance peak in the NIR portion of the spectrum, within the range of 698 and 712 nm (Figure 5g), is the result of scattering from algal cells, pigment and particulate matter in combination with water. The location and height of this peak is a function of chl-a concentration. Peak shifts toward longer wavelengths and increase in height are indications of increased chl-a concentration (Dekker et al., 1991; Gitelson, 1992; Han & Rundquist, 1997; Mittenzwey et al., 1992; Schalles et al., 1998). Reflectance features at wavelengths longer than 750 nm are attributed to organic and non-organic suspended matter concentrations (Han et al., 1994).

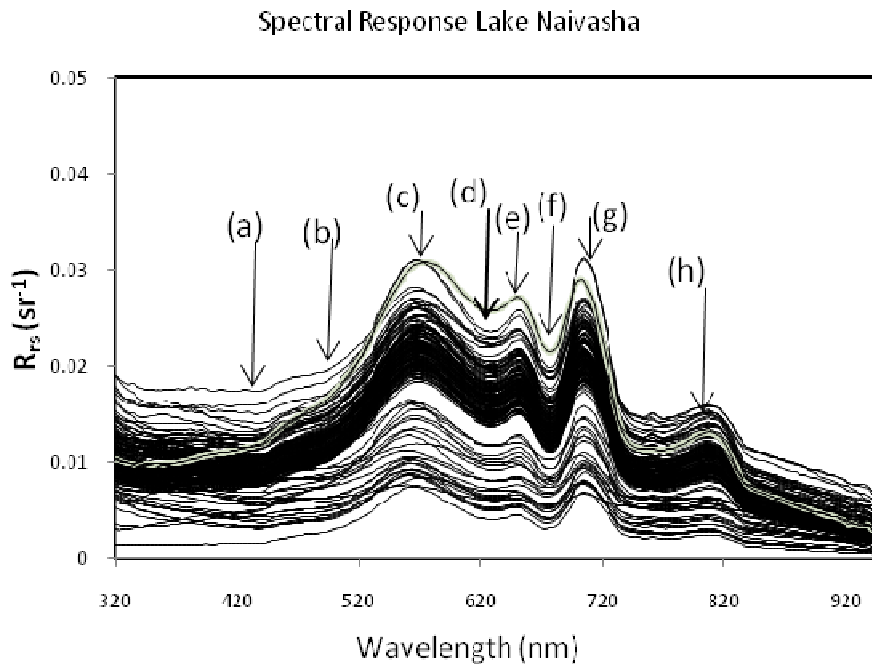
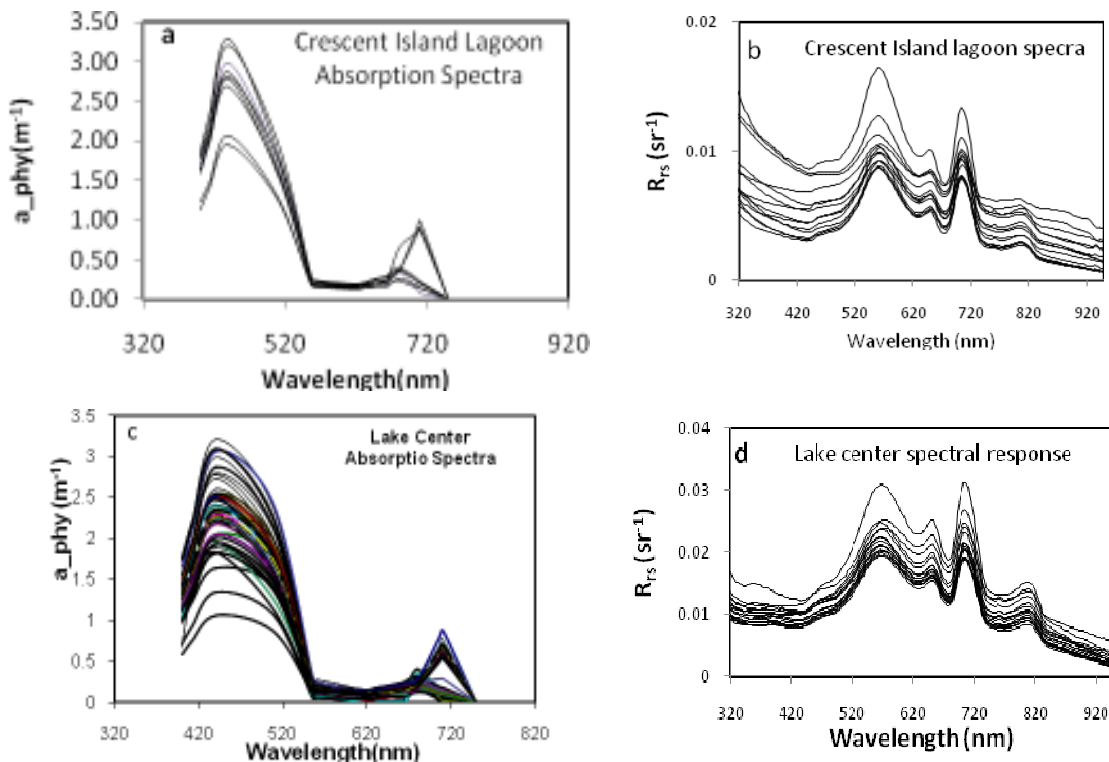


Figure 5. Shows spectral features in the reflectance of Trios-sensor measured from lake Naivasha.

The spectrum from Crescent Island lagoon are shown at the bottom the upper reflectance are from the main lake collected on September 17th through October 3rd, 2010.



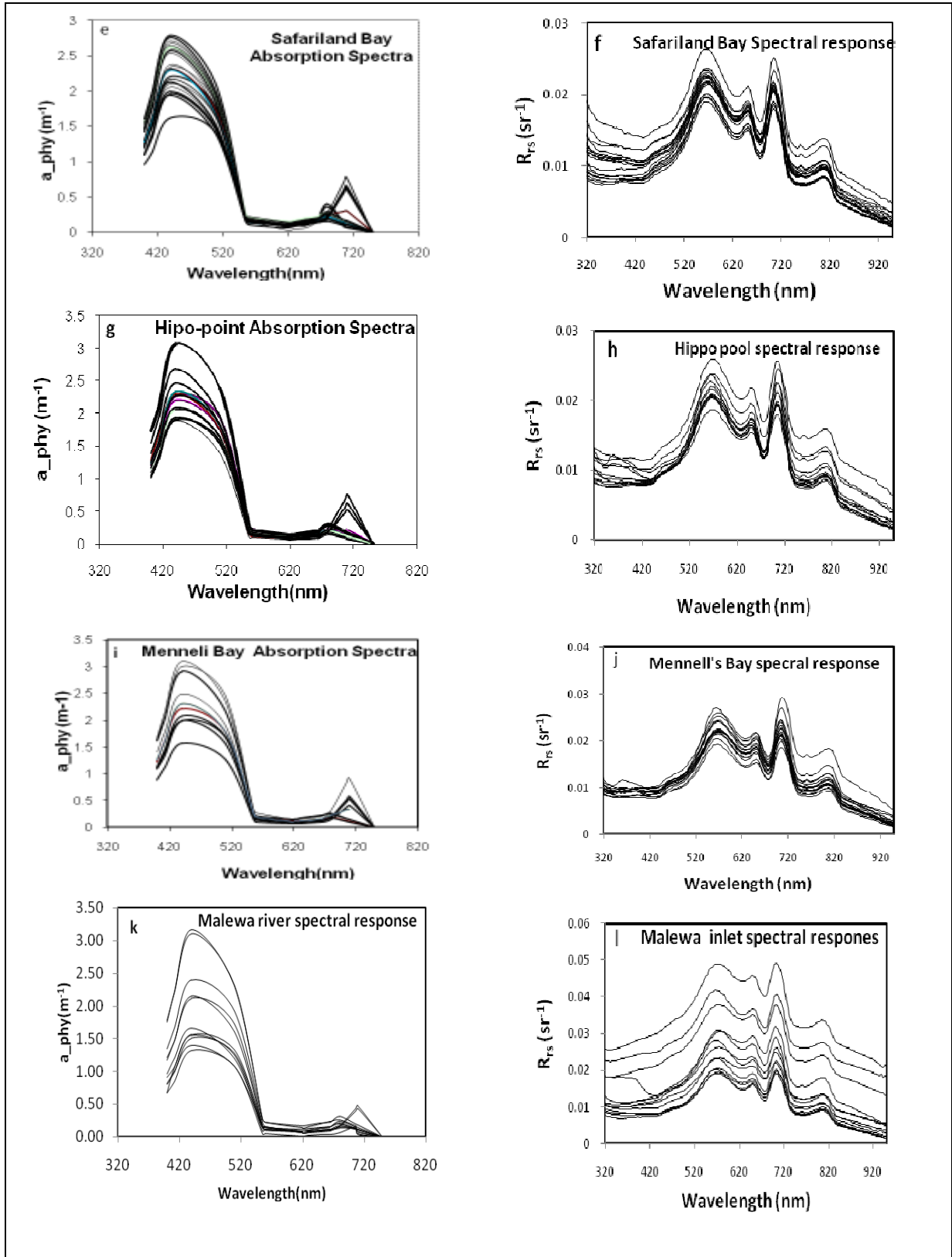


Figure 6. In situ absorption and corresponding reflectance spectra (left and right)

(a, b) absorption and reflectance spectra from Crescent Island (c, d) are absorption and reflectance spectra from the lake centre. (e, f) absorption and reflectance spectra from the Safariland bay. (g, h) Hipo-point absorption and reflectance spectra. (i, j) The Menneli's bay absorption and reflectance spectra. (k, l) absorption and reflectance spectra from the Malewa inlet.

Many factors contribute to the variation in the reflectance peak in the blue and green spectral regions including the coloured dissolved organic matter, non-algal particulate matter and suspended sediments. The reflectance spectra in the red and NIR spectral regions however are less affected by the above mentioned water constituents and are often exploited for chl-a information.

The spectral reflectance values from the Crescent Island lagoon stations (Figure 5) are low ranging from 0.0039sr^{-1} to 0.008sr^{-1} . The averaged minimum red spectral reflectance in the main lake however, was 0.012sr^{-1} , though a lower value of 0.005sr^{-1} is recorded in the lake centre as well. This minimum reflectance values however were not as low as for the Crescent Island lagoon spectra 0.0039sr^{-1} . Variability of spectral reflectance features could manifest high variability in scattering and in CDOM and NAP absorption between samples (Gitelson et al., 2008). The minimum reflectance in the Crescent Island lagoon was associated with maximum chl-a absorption.

The Malewa river inlet absorption and reflectance spectra shows distinct spectral feature different from the other regions. The red spectrophotometric absorption peak around 665 nm for this region is almost indistinguishable (Figure 6k) indicating minimum chl-a absorption or maximum back scattering by suspended sediments (Gitelson, 1992). These stations are at the inlet of the most influential river in Lake Naivasha, Malewa which feeds sediments and other nutrients to the lake. Moreover in the in situ reflectance spectra measured with the Trios-RAMSAS in this region showed high variability in the reflectance magnitude due to reflectance enhancement by increased suspended sediment concentration levels (Gitelson et al., 1993). The Hippo-Point stations (Figure 6g) showed the least variability in the height of the reflectance spectra between the stations indicating relatively stable water constituent. The Menneli's and Safariland bay stations also indicate spectral variability even though not as pronounced as in the Malewa stations. The increase in reflectance height in each of the sub-regions was associated with an increase in the phytoplankton absorption coefficient measured. These variations could also be observed in the absorption maps produced by the three band model (Figure 13).

4.3. Empirical Algorithms used

4.3.1. Three Band Algorithm

Accurate assessment of phytoplankton absorption coefficients in turbid inland waters by means of remote sensing chl-a is challenging due to the optical complexity of case 2 waters (Gitelson et al., 2008). Different bio-optical modelling has been pursued for water quality assessment to eliminate the need for gathering water samples to provide statistical analysis linking phytoplankton concentration to reflectance, thus improving the accuracy of algorithms extended to air and space-borne systems (Randolph et al., 2007, submitted). However, both semi-empirical and bio-optical models require the specific absorption coefficients for algal pigments to be known or to be constant. Unfortunately, the specific absorption coefficient of chl-a is highly variable (Dall'Olmo & Gitelson, 2005b) suggested that certain spectral regions are highly affected by the variability in the chl-a specific absorption coefficient ($a_{\text{chl-a}}^*$) and chl-a fluorescence quantum yield (η), the efficiency at which a cell will emit absorbed light (photons emitted: photons absorbed), introducing high error to the prediction of chl-a from remote sensing reflectance. To resolve this issue, Dall'Olmo and Gitelson (2006) suggested a band tuning method, reducing the requirement for parameterization of the optical properties of natural water constituents by selecting bands that are least affected by $a_{\text{chl-a}}^*$ and η . Based on the hypothesis that bands used in a semi-empirical model for determination of chl-a concentration can be tuned to reduce the sensitivity of the model to variation in the phytoplankton specific absorption coefficient and chlorophyll a fluorescence quantum yield, Dall'Olmo and Gitelson (2005b) presented the following three-band algorithm for chl-a estimation, reducing the standard error of estimation to less than 30%.

According to (Randolph et al., 2007, submitted) the three band model by Dall'Olmo and Gitelson (2005b) can be developed as:

$$a_{chla}(\lambda 1) \propto \alpha \left[\left[R_{rs}^{-1}(\lambda 1) - R_{rs}^{-1}(\lambda 2) \right] \times R_{rs}(\lambda 3) \right] + \beta \dots\dots\dots \text{Equation 17}$$

Where:

α and β are the fitting coefficients

$R_{rs}(\lambda 1)$ = reflectance value at wavelength location $\lambda 1$ most sensitive to pigment absorption (chlorophyll a or phycocyanin), but also affected by particulate material induced scattering and absorption of accessory pigments.

$R_{rs}(\lambda 2)$ = reflectance value at wavelength location $\lambda 2$ that is least sensitive to absorption by the pigment of interest and is most sensitive to absorption by other constituents (correcting for the absorption by other pigments at $\lambda 1$)

$R_{rs}(\lambda 3)$ = reflectance value at wavelength location $\lambda 3$ least affected by absorption of all pigments and therefore used to quantify scattering by water molecules.

The above three-band optical model for obtaining the phytoplankton absorption coefficient (by utilizing the band in the red and NIR region of the spectrum, which is proportional to chl-a absorption) in natural waters requires the selection of three specific wavelength locations based on the sensitivity of that wavelength region on the properties of constituent of interest:

$$a_{phy}(\lambda 1) = m\chi(\lambda 1, \lambda 2, \lambda 3) + b \dots\dots\dots \text{Equation 18}$$

Where:

$a_{phy}(\lambda 1)$ = phytoplankton absorption coefficient at $\lambda 1$.

m = coefficient obtained from regression analysis.

χ = model index values obtained from the reflectance to assess the absorption of a pigment of interest.

b = coefficient obtained from regression analysis

The first band location ($\lambda 1$) is selected as the spectral feature most sensitive to chlorophyll a pigment absorption:

$$R_{rs}^{-1}(\lambda 1) \propto \frac{Q}{f} \frac{a_{chla}(\lambda 1) + a_{TD}(\lambda 1) + a_w(\lambda 1) + b_b}{b_b} \dots\dots\dots \text{Equation 19}$$

Where:

R_{rs}^{-1} = the reciprocal of the remote sensing reflectance function as defined by Gordon et al.(1975) (Eqn.1)

$(\lambda 1)$ = spectral region chosen as most sensitive to chl-a absorption

a_{Chla} = chlorophyll a absorption coefficient at the specified wavelength location.

a_{TD} = total absorption coefficient for the non-algal particles (tripton) and coloured dissolved organic matter (a_{CDOM}) combined (sometimes called a_{NAP}).

$a_w(\lambda 1)$ = pure water absorption coefficient at the specified wavelength location

b_b = total backscattering coefficient

f : Q = a function of the sun and viewing angles

The second spectral region is selected as the wavelength where absorption of non-algal particles and CDOM is equal to the absorption of the first spectral region and absorption by chl-a is minimal. Because the absorption efficiency of CDOM and NAP decreases as wavelength increases, $\lambda 2$ is chosen to be > 700 nm.

Tuning for $\lambda 2$ is written as:

$$R_{rs}^{-1}(\lambda 1) - R_{rs}^{-1}(\lambda 2) \propto \frac{Q}{f} \frac{a_{chla}(\lambda 1) + a_w(\lambda 1) - a_w(\lambda 2)}{b_b} \dots\dots\dots \text{Equation 20}$$

Where:

$a_{Chla}(\lambda 1)$ = chlorophyll a absorption coefficient at the specified wavelength location

$a_w(\lambda_1)$ = pure water absorption coefficient at the specified wavelength locations

Wavelength location λ_3 is selected according to the location least affected by absorption of all pigments, therefore absorption at λ_3 can be attributed solely to that of pure water and can be used to quantify scattering by water molecules. Reflectance at λ_3 is proportional to the product of f: Q ratio and total backscattering, (Eqn.20) written as:

$$a_{chla}(\lambda_1) \propto [R_{rs}^{-1}(\lambda_1) - R_{rs}^{-1}(\lambda_2)] \times R_{rs}(\lambda_3) \dots\dots\dots \text{Equation 21}$$

The following steps are employed for adoption of the initial spectral regions:

(1) Tuning of λ_1 by use of the initial band locations $\lambda_2=710$ nm and $\lambda_3=750$ nm and a moving location for λ_1 between 400 and 800 nm, thus:

$$a_{chla}(\lambda_1) \propto [R_{rs}^{-1}(400 < \lambda_1 < 800) - R_{rs}^{-1}(710)] \times R_{rs}(750) \text{ regressed against chl-a absorption coefficients in the wavelength range (400 to 800nm) to obtain the lowest standard error of estimation.}$$

(2) Tuning of λ_2 by use of the tuned λ_1 location (from step 1) and initial $\lambda_3=750$ nm and a moving location for λ_2 between 700 and 750 nm, thus:

$$a_{chla}(\lambda_1) \propto [R_{rs}^{-1}(\lambda_1) - R_{rs}^{-1}(700 < \lambda_2 < 750)] \times R_{rs}(750) \text{ regressed against Chl-a absorption coefficient to obtain the lowest standard error of estimation.}$$

(3) Tuning of λ_3 by use of the tuned λ_1 and λ_2 locations and a moving location for λ_3 between 730 and 750 nm, thus:

$$a_{chla}(\lambda_1) \propto [R_{rs}^{-1}(\lambda_1) - R_{rs}^{-1}(\lambda_2)] \times R_{rs}(730 < \lambda_3 < 750) \text{ regressed against chl-a absorption coefficients to obtain the lowest standard error of estimation.}$$

(4) Verification of location λ_1 by use of a tuned λ_2 and λ_3 and a moving λ_1 regressed against Ch-a absorption coefficients to obtain the lowest standard error of estimation, giving the final algorithm indicated in (Eqn.17):

Dall’Olmo and Gitelson (2006) suggest that, although the tuning technique and coefficients used in this model are dependent on the optical composition of the water on which it was built, the large range of constituent concentrations and optical properties included in the model derivation suggest that it could be extended to similar systems. The phytoplankton absorption coefficient could be obtained by utilizing a band in the red region which is proportional to chl-a concentration in natural waters. Reflectance values at wavelength location λ_2 could be tuned to that is least sensitive to absorption by phycocyanin and potentially most sensitive to absorption by other constituents (correcting for the absorption by other pigments at λ_1).

Similarly in order to find optimal positions of λ_1 , λ_2 and λ_3 and the width of each band in the three band model, the model was tuned according to the optical property of the water in Lake Naivasha. The final values of band widths were selected at the minimum RMSE between the measured and derived a_{phy} as:

Band1 660 through 670 nm, band2 700 through 730 nm and band3 was selected between 740 and 760 nm.

4.3.2. Synthetic Chlorophyll Index

Although the current generation of the satellite ocean colour sensors have large number of wave bands in the visible spectral range, it is still difficult to develop retrieval algorithms using remote sensing signals (Shen et al., 2010) because the water constituents vary independently. Reflectance spectrum of water bodies with high suspended sediment concentration levels is enhanced due to high back scattering by the sediments resulting in an invalid flag or overestimation of chl-a from remote sensing (Morel & Bélanger, 2006). To improve the accuracy of MERIS chl-a estimates in such turbid lakes, (Shen et al., 2010) devised an algorithm (Synthetic Chlorophyll Index, SCI) for extracting chlorophyll information by minimizing the sediment influence on the remote sensing reflectance spectrum. This algorithm takes the variability of spectral reflectance features of chl-a and the sediments into account synthetically by introducing two parameters H_{chl} and H_{Δ} for the SCI. The H_{chl} is the height of the red chl-a absorption dip in the spectrum of MERIS while H_{Δ} is the absorption feature around 620nm introduced due to suspended sediments or other accessory pigments.

$$H_{chl} = \left[R_{rs}(\lambda_1) + \frac{\lambda_2 - \lambda_1}{\lambda_3 - \lambda_1} (R_{rs}(\lambda_3) - R_{rs}(\lambda_1)) \right] - R_{rs}(\lambda_2) \dots \dots \dots \text{Equation 22}$$

$$H_{\Delta} = R_{rs}(\lambda_2) - \left[R_{rs}(\lambda_4) + \frac{\lambda_2 - \lambda_4}{\lambda_3 - \lambda_4} (R_{rs}(\lambda_3) - R_{rs}(\lambda_4)) \right] \dots \dots \dots \text{Equation 23}$$

Where: $\lambda_1, \lambda_2, \lambda_3$ and λ_4 are MERIS bands 620nm, 665nm, 681nm and 560 nm respectively. These parameters can be simplified according to their weighted sum as:

$$H_{chl} = [0.74R_{rs}(681) + 0.26R_{rs}(620)] - R_{rs}(665) \dots \dots \dots \text{Equation 24}$$

$$H_{\Delta} = R_{rs}(620) - 0.5[R_{rs}(560) + R_{rs}(681)] \dots \dots \dots \text{Equation 25}$$

H_{chl} and H_{Δ} are less than zero if and only if $R_{rs}(665)$ is greater than $[0.74R_{rs}(681) + 0.26R_{rs}(620)]$ and $R_{rs}(620)$ is less than $[0.5(R_{rs}(560) + R_{rs}(681))]$ respectively. Shen et al.(2010) has demonstrated that R_{rs} at 665nm is generally below the baseline connecting the R_{rs} at 620nm and R_{rs} at 680nm leading to positive H_{chl} values. Negative H_{chl} are interpreted as the lack of chl-a or presence of high SSC.

This band positions upon which the model was originally developed resulted in a negative value of H_{chl} for all the spectra due to the dynamic nature of the peak and dip positions of the in-situ Trios reflectance measurement. The dip and peak at 665nm and 680nm of the MERIS spectrum up on which the model was initially set corresponds to the peak and dip at 676 nm and 706 nm respectively in the Trios spectra. To account for this effect the dynamic nature of the peak and dip positions were taken into consideration and the model was calibrated by taking the local peaks and dips near 560nm, 626nm, 676nm and 706nm for $\lambda_4, \lambda_1, \lambda_2$ and λ_3 respectively (Figure 7).

The SCI index was computed as a difference of the above parameters and was used in retrieving phytoplankton absorption coefficient.

$$SCI = H_{chl} - H_{\Delta} \dots \dots \dots \text{Equation 26}$$

The in-situ spectrophotometric chl-a absorption values, and the H_{chl} and H_{Δ} parameters, were used determine the fitting coefficients on the SCI algorithm by a linear regression and the modified algorithm was applied to MERIS data retrieval chl-a information.

$$SCI = \alpha_1 [C_{chla}]^2 + \alpha_2 [C_{chla}] + \alpha_3 \dots \dots \dots \text{Equation 27}$$

Since Chl-a concentration is a function of its absorption; the above expression can be rewritten as:

$$SCI = \alpha_1 [a_{phy}(\lambda)]^2 + \alpha_2 [a_{phy}(\lambda)] + \alpha_3 \dots \dots \dots \text{Equation 28}$$

Where: $\alpha_1, \alpha_2, \alpha_3$ in SCI are fitting coefficients and $a_{phy}(\lambda)$ is phytoplankton absorption coefficient at the specified wavelength. After determining the fitting constants from the field radiometric and spectrophotometric measurements, chl-a absorption was validated against an independent in-situ dataset and MERIS match up data.

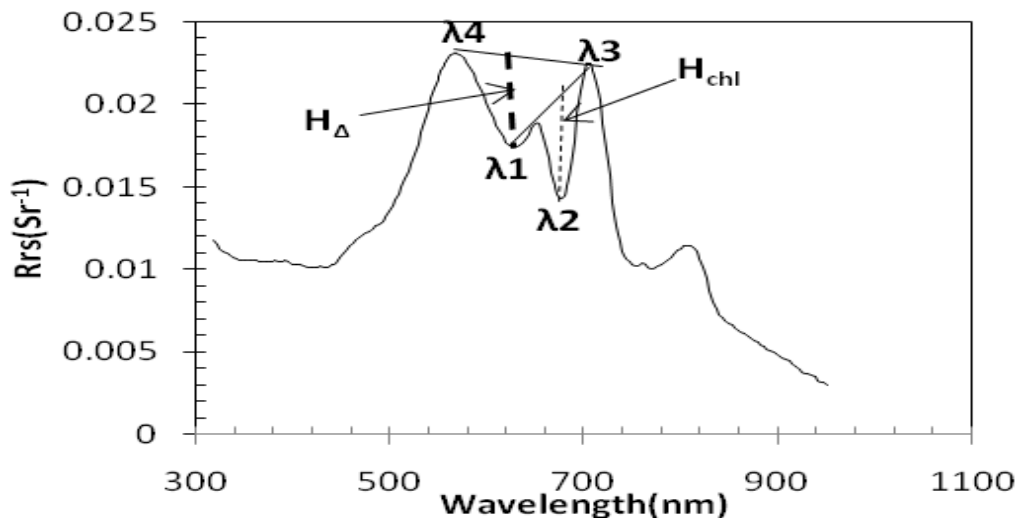


Figure 7. Schematic representation of SCI algorithm.

It can be seen from the above figure the spectral positions of the peaks and dips used in the SCI model. Wavelengths 560nm, 626nm, 676 nm and 706 nm indicated by (λ_4 , λ_1 , λ_2 , and λ_3) are from the Trios-sensor which were applied in the model calibration.

4.3.3. Fluorescence Line Height

During daytime, phytoplankton assemblages in the surface waters emit low but detectable levels of chlorophyll fluorescence around 683 nm (Laney et al., 2005). Remote sensing of solar-induced phytoplankton chlorophyll fluorescence emission around 683 nm has had recurring study over the past several decades (Hoge et al., 2003). Although natural chlorophyll fluorescence is affected by complex physiological processes, its variability in natural phytoplankton assemblages is not random. Systematic changes are often associated with physical features like up welling eddies, frontal circulation features and meandering jets (Abbott et al., 2000). The Moderate Resolution Imaging Spectroradiometer MODIS sensor on the Terra spacecraft launched on 17th December 1999 was the first satellite realization of the chlorophyll fluorescence line height FLH method. The European Space Agency's Medium Resolution Imaging Spectrometer, or MERIS, carries similar technology, as does NASA's MODIS, recently launched 4th May 2002 aboard the Aqua spacecraft. In this research the FLH base line method is computed from an in-situ spectrophotometer and hyperspectral data and validated with concurrent MERIS data for phytoplankton chlorophyll fluorescence line height retrievals from remote sensing.

Chlorophyll fluorescence, as introduced by Lorenzen (1966), is commonly used as an indicator for phytoplankton biomass, despite the poor relationship between the Chl a concentration and the amount of fluorescence emitted. The amount of fluorescence emitted is, besides on the Chl-a concentration, dependent on the photosynthetic available radiation (PAR), the absorptive properties of the phytoplankton, the extent to which the emitted fluorescence is reabsorbed, and the fluorescence yield (Babin et al., 1996). Algorithms have been developed to estimate surface ocean chlorophyll from remotely sensed natural fluorescence (IOCCG 1999; Hoge et al., 2003) such algorithms may be particularly useful in Case II waters, where the presence of non-phytoplankton scatterers and absorbers degrade the standard radiance reflectance algorithms for chlorophyll.

Fluorescence line height (FLH) calculated as the reflectance in band 8 (681 nm) above a baseline formed by linear interpolation between the reflectance in bands 7 (665 nm) and 9 (709 nm) (linear baseline algorithm, (Gower et al. 2004). This signal is a measure of the fluorescence of chl-a, which is stimulated by sun- and skylight and is emitted as a roughly Gaussian shaped spectral feature centred at 685 nm. The fluorescence is an indicator of chl-a concentration, but with variation in specific fluorescence with species,

increasing saturation for pigment concentrations in the range 1–30 mgm⁻³, and loss of the FLH signal at higher concentrations (Gower et al., 2005) (Figure 8).

In his study of chl-a fluorescence (Gower et al., 2005), found that water reflectance is high at wavelengths shorter than 500 nm for chl-a concentration of less than 1 mgm⁻³ (blue water), but drops as chl-a concentration increases, giving a peak near 560 nm (green water). Chl-a fluorescence produces a narrower peak at 685 nm for chl-a concentration up to about 30 mgm⁻³, but above this concentration the absorption by water and chl-a pigments combine to shift the peak to longer wavelengths (706 nm at 300 mgm⁻³) (Figure 8)

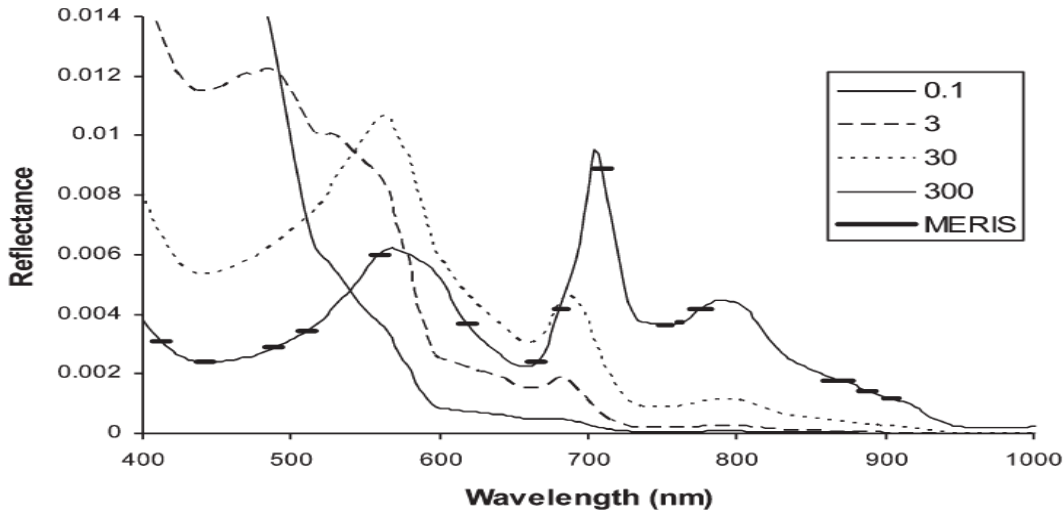


Figure 8. Water reflectance spectra for chlorophyll a concentrations of 0.1, 3, 30 and 300 mgm⁻³,

showing the fluorescence peak at 685nm for lower chlorophyll concentrations and the peak in the wavelength range 700–710nm for chlorophyll a concentrations above about 100 mgm⁻³. Black horizontal bars on the spectrum for chlorophyll a concentrations = 300mgm⁻³ show how the positions and widths of spectral bands in the MERIS baseline band-set allow this peak to be detected, and its height measured adopted from (Gower et al., 2005).

Computation of the chl-a fluorescence from the reflectance spectra measured in lake Naivasha at bands 7, 8, and 9 using the FLH base line method ended up in a negative result due to loss of the fluorescence peak around 685 nm which could be related to its higher chl-a concentration level (Gower et al., 2005). This can be elaborated from the in-situ reflectance spectra measured in lake Naivasha, where the peak has shifted towards longer wave length (~706 nm) as a result of the absorption by increased chl-a concentration level and water.

The FLH derived from the TRIOS sensors above-water reflectance measurements was calculated as:

$$FLH = Rrs(B_8) - Rrs(B_9) - \frac{[(Rrs(B_7) - Rrs(B_9)) \times (B_9 - B_8)]}{[B_9 - B_7]} \dots\dots\dots \text{Equation 29}$$

Where: Rrs (B7), Rrs (B8), Rrs (B9) are the remote sensing reflectance at MERIS bands 7, 8, and 9. The FLH index values obtained from the (Eqn.29) were negative for all the spectra indicating a lose or shift of the FLH signal around 685 nm.

Similar to the FLH technique the chl-a information was computed according to the Trios spectral feature from lake Naivasha.

To account for the low FLH signal and shift of the peak to wards longer wavelength, the chl-a information was computed from reflectance at band 9 (709nm) above that base line connecting bands 8

and 10 at (681nm and 753 nm) which is referred to as the Maximum Chlorophyll Index (MCI) in MERIS documents.

The MCI algorithm (Figure 9) computed in a similar way as the FLH, but using bands 8, 9 and 10 (681, 709 and 753 nm) of the water leaving reflectance from Trios sensor. This computation gives a Maximum Chlorophyll Index (MCI) which will tend to be negative where FLH is high and a reflectance peak occurs near 685 nm, but positive where the reflectance peak has shifted to longer wavelengths, up to about 705 nm. The 709 nm band of MERIS is centred at a slightly longer wavelength than the peak in the Trios (706 nm), but covers the range 704–714 nm.

The empirical MCI method used in this study relies on three independent measurements: one near the maximum of Chl-a fluorescence emission (683–685 nm) which is band 9 (708.329nm) and two reference bands 8 and 10 (680.821nm and 753.371nm) to define a ‘baseline’ below the peak.

$$MCI = Rrs(B_9) - Rrs(B_{10}) - \frac{[(Rrs(B_8) - Rrs(B_{10})) \times (B_{10} - B_9)]}{[B_{10} - B_8]} \dots\dots\dots \text{Equation 30}$$

The MCI index value was then regressed against the red in-situ chl-a absorption coefficient to determine the best coefficient for the determination of phytoplankton absorption coefficient of lake Naivasha and a weak quadratic polynomial relation (

Figure 10d) was established between the index value and the in-situ absorption coefficients as:

$$MCI = \alpha[a_{phy}(\lambda)]^2 + \beta[a_{phy}(\lambda)] + \gamma \dots\dots\dots \text{Equation 31}$$

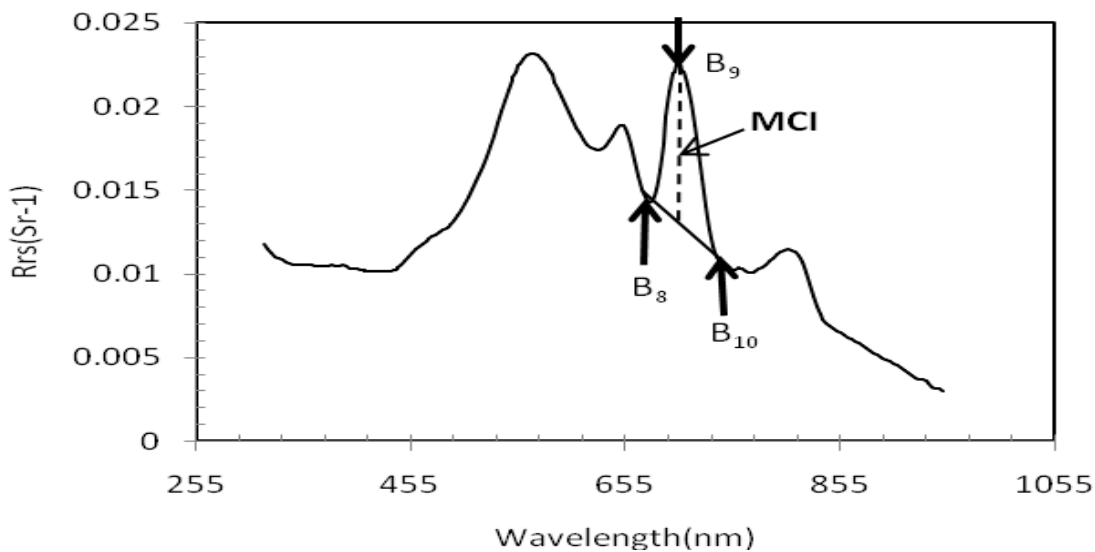


Figure 9 Schematic representation of MCI algorithm.

The above figure shows the relative transmittance of MERIS bands 8, 9, and 10 labelled B8, B9, B10. The baseline for MCI measurement is established by a straight line between the reflectance observed in bands 8 and 10. MCI is the reflectance within band 9 that is above the baseline value.

4.3.4. Algorithm Calibration and Validation

Datasets with concurrent radiometric and laboratory measurement were divided into calibration and validation datasets and algorithms were calibrated using statistical least square regression method. Calibration datasets are chosen every other station for fair distribution of values. Out of the 137 measurements only 90 stations were selected for analysis due to error and noises introduced in the

measurement from various sources. Model calibration was done with half of this dataset (48 stations) for both models and were validated with rest of the measurement (42 station) Having well distributed calibration dataset of wider value range helps in validating against an independent dataset with good coefficient of determination. Satellite data validation were performed with in situ data collected within $\pm 2-3$ hr of the satellite overpass (Bailey & Werdell, 2006). This however has led us to very few matching data pairs due to frequent cloud cover, measurement delays or other inconveniences. In this research the match-up date validation was done with 20 stations from three MERIS match-up date images (Table 3) for measurements within the above stated range of over pass time offsets. The statistical summary of the calibration and validation results of the models is presented in (Table 7).

The SCI and MCI algorithms were tested to use bands of maximum and minimum reflectance and absorption that correspond to algal optical properties, while the 3Band model was tested at wavelength band ranges instead of single band values to improve algorithm performance.

The maximum and minimum reflectance values of the selected bands were used within the specified ranges given in (Table 4) Regression plots of algorithm index values against analytically measured chl-a absorption coefficient were analyzed to develop the best fit coefficients to predict chl-a absorption for lake Naivasha (Figure 10). The coefficient of determination and root mean square error (RMSE) were calculated for each model (Table 6).

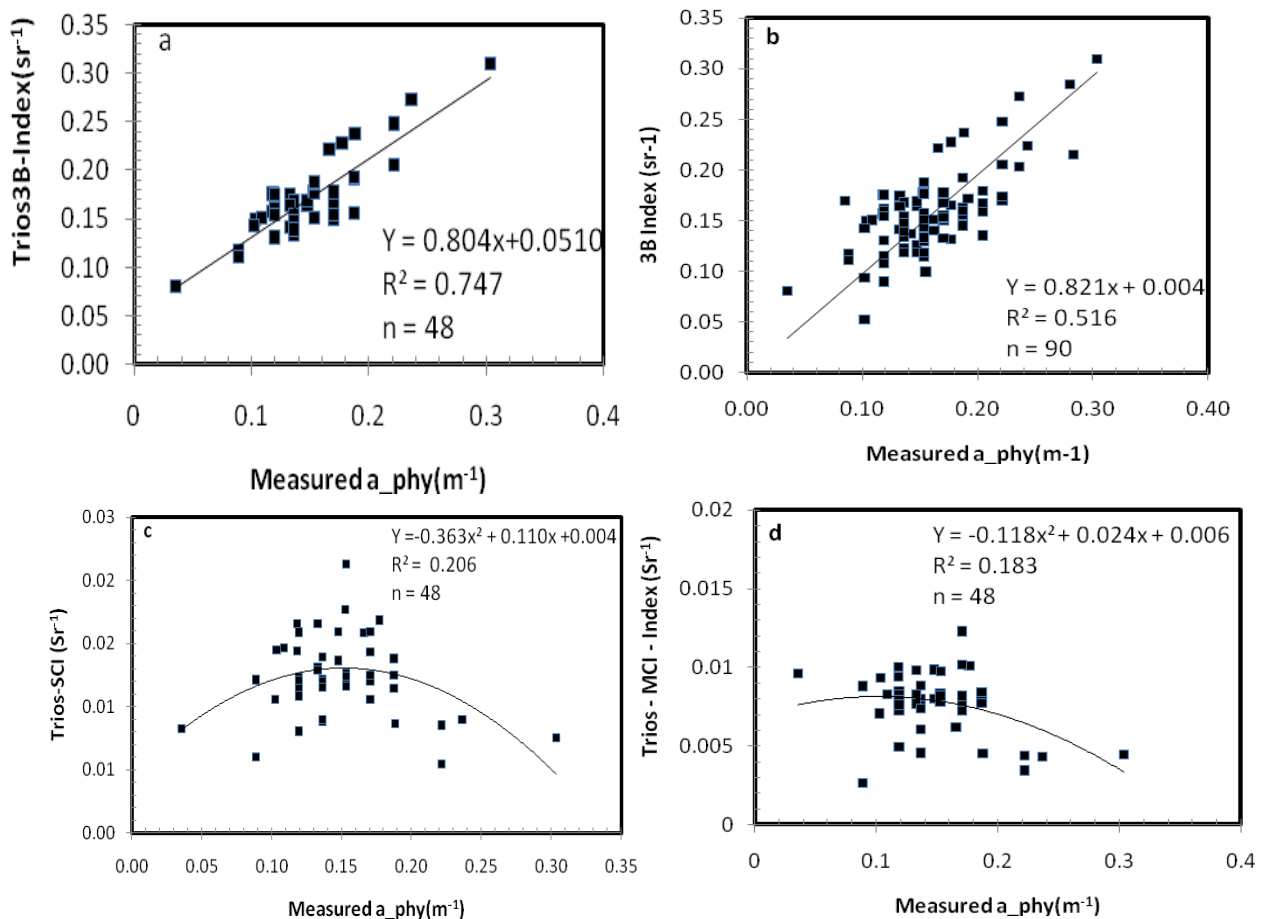


Figure 10 . Model Calibration with in-situ measured absorption coefficient.

(a) 3B model calibration plot computed from Trios reflectance at bands 7, 9, and 10 and in-situ absorption coefficients. (b) 3B calibration for the combined (calibration and validation) datasets ($n=90$) against in-situ chl-a absorption coefficients (c) SCI model calibration plot computed from Trios reflectance at bands 5, 6,

7 and 8 and in-situ absorption coefficients. (d) MCI model calibration plot computed from Trios reflectance at bands 8, 9, 10 and in-situ absorption coefficients.

Correlation of the in-situ phytoplankton absorption with the SCI index value revealed a weak quadratic polynomial function with a coefficient of determination and RMSE of 0.21 and 0.111. Similarly the MCI algorithm resulted in a weak polynomial quadratic function with a coefficient of determination and RMSE of 0.18 and 0.146 respectively (Table 6).

4.4. Measuring Algorithm Accuracy and Robustness

The algorithms’ accuracy in predicting phytoplankton absorption coefficients in lake Naivasha was tested through a least-squares regression. The coefficients, and their corresponding RMSE and r² values (Table 6) obtained from the linear least-squares regression analysis of measured versus estimated absorptions of phytoplankton pigments describe the algorithms’ fit. Overall model performance was reported using the root-mean-square error (RMSE) of the estimated phytoplankton absorption:

$$RMSE = \sqrt{\frac{\sum_{i=1}^n (Y_i - X_i)^2}{(n-2)}} \dots\dots\dots \text{Equation 28}$$

Where:

Y_i= estimated concentration of pigment i

X_i= measured concentration of pigment i

n = number of observations

To test the robustness of the algorithms, the data was divided into two sets, including a calibration and validation datasets (n=48 and n=42) respectively. Analyzed sampling sites were divided into half by selecting every other sampling site, resulting in the calibration dataset and the remaining data was used for validation. Chl-a absorption, was then derived for the validation dataset by the application of the regression equation obtained from the linear least-squares regression of the index value from each model and the measured chl-a absorption from the calibration dataset.

Model Calibration Summary				
Model	n	r ²	RMSE	Equation
3B	48	0.747	0.04208	Y = 0.804X+0.051
SCI	48	0.206	0.11126	Y = -0.0363X ² +0.110X+0.004
MCI	48	0.183	0.14607	Y = -0.167X ² +0.039X+0.006

Table 6. Calibration summary of the three models .

Least squared linear regression of model index values derived from the insitue measured Trios reflectance and the in-stue spectrophotometric chl-a absorption coefficient.

Validation of the calibrated algorithms was done using an independent data-set (the Trios and MERIS reflectanc n=42) from the lake and the best fitting coefficients obtained from the calibration equations were used to derive back the chl-a absorption coefficient measured in-situ and the derived absorption coefficients were reggrssed against the in-situ measured chl-a absorption coefficient to evaluate the algorithm performance and accuracy using r² and RMSE values (Table 7). Only the 3B model showed a strong linear relationship for an aggregate dataset (n=42) of in-situ measured absorption coefficients whereas both the SCI and MCI algorithms couldn’t hold for the aggregate dataset (n=42). It was found that the SCI algorithm fails at validating against stations with SCI index values above 0.0123sr⁻¹ and chl-a absorption of greater than 0.2m⁻¹ and were validated against half of the independent dataset though the poor perfomance is still not improved (Table 7). Similarly the MCI algorithm was validated only for stations with index values of between 0.0061 sr⁻¹ to 0.0083sr⁻¹.

Trios RAMSAS- Validation Performance					MERIS Validation Performance			
Model	n	r ²	RMSE	Equation	n	r ²	RMSE	Equation
3B	42	0.838	0.058	Y=1.094X-0.070	20	0.642	0.648551	Y=14.48X-0.923
SCI	19	0.486	0.139	Y = 0.116X-0.006				
MCI	19	0.213	0.151	Y= 0.010X+0.0003				

Table 7 Performance summary of the three algorithms.

Performance summary of models at estimating chl-a absorption coefficient of lake Naivasha from in-situ Trios-sensor and MERIS data. Included are the number of samples used in the validation (n), the linear equation of the validation plot, r² and RMSE for both the in-situ and MERIS validation.

Due to their poor performance the SCI and MCI models were not validated for MERIS and only the 3B model showed a strong linear relationship both for the Trios and MERIS derived reflectance spectra and hence from hereafter only the results of 3B will be shown and discuss though the results of SCI and MCI will be shown for compariso

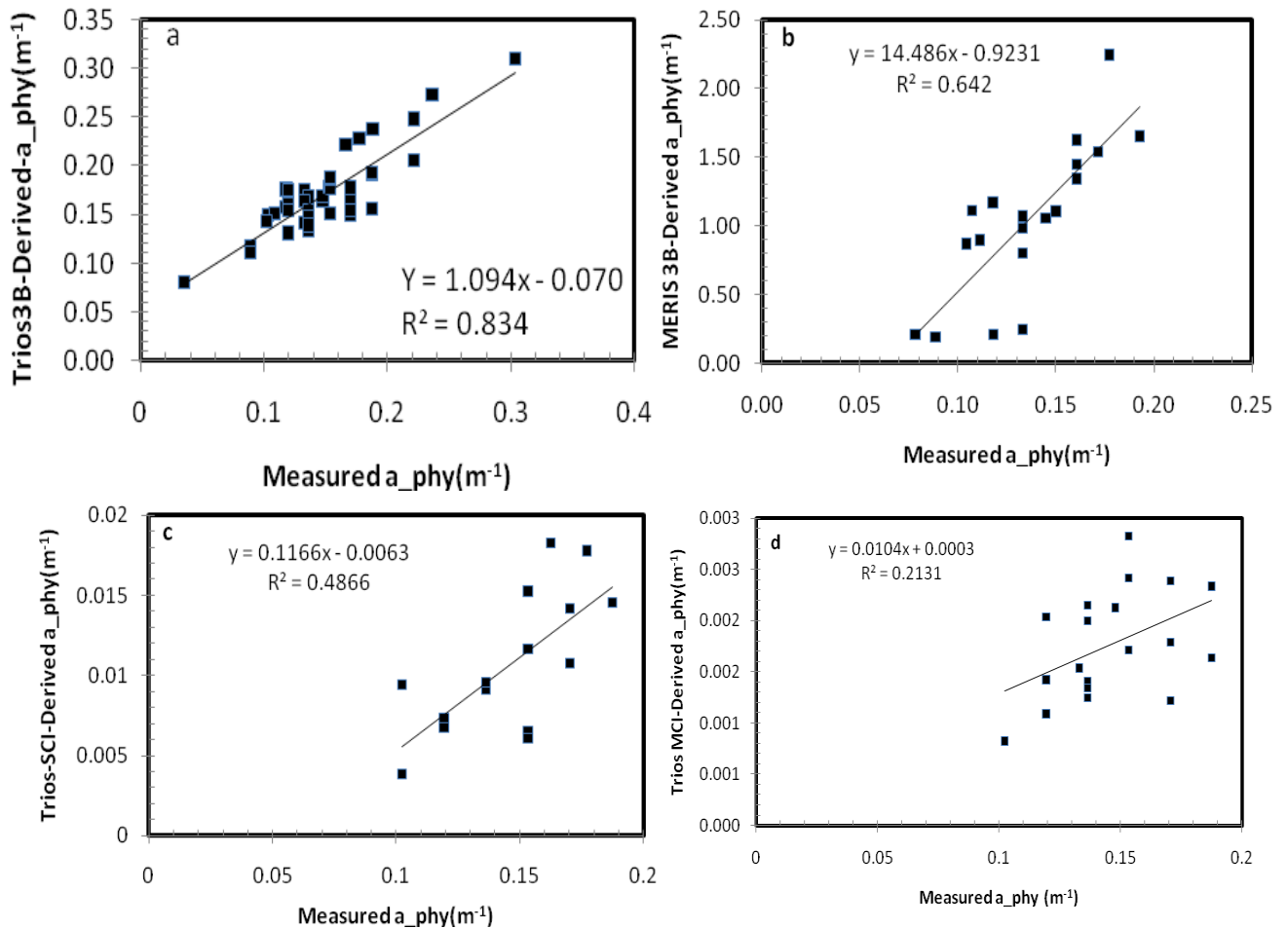


Figure 11. Validation results of the three models against in-situ measured a-phy plotted to the same scale. (a, b) 3B validation of chl-a absorption estimation from in-situ Trios and remote sensing (MERIS) dataset (n= 42 and n=19) for the Trios and MERIS respectively. (c) Shows the SCI validation result of estimation of chl-a absorption versus in situ measured ch-a absorption for stations with SCI index values of less than 0.0123sr⁻¹(n=19). (d) Shows the MCI validation result of estimation of chl-a absorption versus in situ measured ch-a absorption for stations with MCI index values between 0.0061 sr⁻¹ to 0.0083sr⁻¹ (n=19).

5. RESULTS AND DISCUSSIONS

The in-situ chl-a absorption data from lake Naivasha showed a large variation in the magnitude and position of the red spectral absorption coefficient near 665nm. The highest and lowest chl-a absorption coefficients were measured in the Crescent Island lagoon and Malewa river inlet respectively. The in-situ spectrophotometric absorption coefficient measurement also showed variation in the position of the red absorption peak between 680nm and 710nm with a corresponding increase in peak magnitude. The magnitude of absorption for spectra with peak position at 680 nm varied from 0.1662 to 0.4021 per meter and the absorption peak of spectra with peak position at 710nm varied from 0.2727 to 1.1817 per meter (Table 2) The increase in the peak height was accompanied by a shift in the peak position towards longer wavelength which could be related to an increase in chlorophyll concentration (Gitelson, 1992). In his experiment in turbid in land and coastal water bodies, Gitelson (1992) found that the peak position for chl-a concentration of less than 3 mg/m³ was observed at 680 - 683nm and it shifted to a longer wave length reaching 715nm for chl-a concentration of more than 100 mg/m³.

Comparison of model out puts suggest that the three band algorithm, compared to the SCI and MCI algorithms, is more efficient at accounting the small variability in chl-a pigment absorption coefficients, likely because it utilizes information about the NIR feature as a whole, rather than only in a single band.

Model performance was evaluated by comparing the model outputs from the in-situ Trios-sensor and MERIS water leaving reflectance with the in-situ measured chl-a absorption coefficient. The three band model showed a strong linear relationship with higher coefficient of determination and low RMSE values.

The coefficient of determination and RMSE value of 3B model as indicated in (Table 7) was (0.838, 0.057786 and 0.642, 0.64855) for an aggregate dataset of 42 and 19 for the Trios and MERIS sensors respectively. To test robustness and accuracy of models at estimating chl-a, validation of the calibrated algorithms was performed using an independent data-set (the Trios and MERIS reflectance n=42) and the best fit coefficients obtained from the calibration equations were used to derive back the chl-a absorption coefficient measured in-situ. The derived chl-a absorption coefficients were regressed against the in-situ measured chl-a absorption coefficient to evaluate the algorithm performance and accuracy using r² and RMSE values (Table 7). Only the 3B model showed a strong linear relationship for an aggregate dataset (n=42) between in-situ measured absorption coefficients and derived chl-a absorption, whereas the SCI and MCI algorithms couldn't hold for the aggregate dataset (n=42). It was found that the SCI algorithm fails at validating against stations with SCI index values above 0.0123sr⁻¹ and chl-a absorption of greater than 0.2 m⁻¹ and were validated against half of the independent dataset though the poor performance is still not improved (Table 7). Similarly the MCI algorithm was validated only for stations with index values of between 0.0061 sr⁻¹ to 0.0083sr⁻¹.

Despite the fact that the SCI model was developed and tested for extracting chl-a information in highly turbid water bodies containing high SSC level (> 100 mgm⁻³) by taking in to account the variability of spectral reflectance features and sediment synthetically, it was found to under-perform at characterizing chl-a information of lake Naivasha. The poor performance of this model at estimating chl-a absorption in lake Naivasha could be attributed to the higher chl-a content. The SSC level of Lake Naivasha is not more than 100 mgm⁻³ (Kebede, 2011) which is not as high as the model was initially tested. This could be elaborated by the fact that the model is failing at estimating chl-a for stations with index value of greater than 0.0123 sr⁻¹ which is a lower value for the lake. The higher SCI index value is due to high H_{chl} value (Eqn.22) obtained from reflectance enhancement at 706 nm from Trios sensor due to high backscattering from algal cells and suspended sediments which is beyond the predictive power of the model. Farther analysis and mapping of chl-a was done using the modified and accurate 3B algorithm by Gitelson et, al. after fixing the fitting coefficients for the prediction of chl-a absorption in the lake.

Model residual analysis have showed that the three band model was associated with an overestimation of chl-a absorption in all of the sub-regions analyzed resulting in a negative residual whereas results the MCI and SCI were associated with underestimation of phytoplankton absorption coefficients resulting in a positive residual.

Model out puts of higher chl-a absorption in the Crescent Island lagoon was in agreement with the in-situ absorption measurement, though higher levels of suspended detritus material and floating green to greyish rafts of phytoplankton and leafed plants were observed in the main lake. This can be attributed to the physiological condition of the phytoplankton communities present in both lakes in which the bloom in the Crescent Island lagoon is more active than the counterpart in the main lake. When a bloom event is at its verge of development the algal cells start disintegrating decreasing the photosynthetic activity and much of the absorbed light will be re-emitted as fluorescence instead of being utilized for photosynthesis. Generally speaking, the more efficiently the phytoplankton utilizes the absorbed light for photosynthesis, the less of the absorbed light is re-emitted as fluorescence and hence higher chl-a absorption coefficient readings.

In attempt to investigate the spatial distribution of phytoplankton in the lake, the data was analyzed by dividing the main lake stations into five sub-regions based on geographic locations. Model results of absorption coefficient have showed spatial variations in the phytoplankton absorption coefficient which is also evident from the in-situ chl-a absorption coefficient measurements (Figure 12). The lowest chl-a absorption value was recorded at the Malewa river inlet due to high light inhibiting suspended sediment load from the river which was evident from the minimum sechi disc depth value of 0.22m.

Long term temporal variations of phytoplankton distribution could be analyzed with help of this algorithm provided that images of the lake for the required period of time are available. Previous studies based on physical and biological investigations have demonstrated that there is temporal variation of phytoplankton in lake Naivasha. Progressive increase of phytoplankton distribution has been reported by (Harper, 1992) as a result of nutrient increase caused by a decline in water level and papyrus swamp clearance for agriculture.

This comparison gives an understanding of the application of empirical algorithms of chl-a absorption and fluorescence on optically turbid inland lakes. The accuracy of the resulting calibration and validation of the chl-a absorption for both models was compromised by errors in deriving the level 2 product, especially those introduced by atmospheric correction and the laboratory spectrophotometric measurement which was consistently affected by chl-a degradation products.

Absorption maps were produced by the three band model revealed the variation in the phytoplankton distribution and can be applied in monitoring Lake Naivasha in space and time to some degree of success. It can be observed from map that the chl-a absorption increases from north to the south and east as the SSC level decreases offshore of the Malewa river mouth because of the increase in the amount of sunlight penetrating the water away from the river mouth.

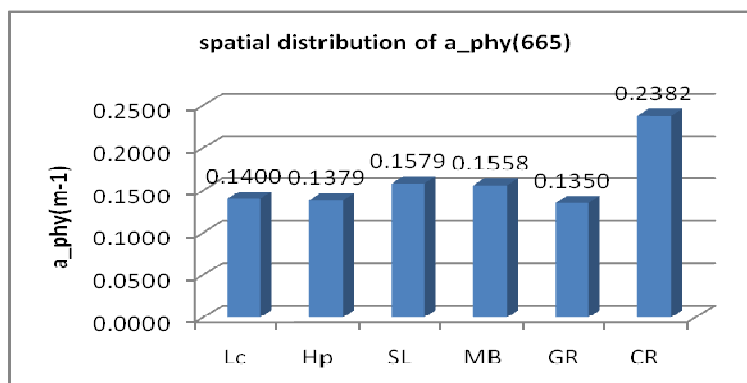


Figure 12. Averaged in-situ absorption coefficient at 665 nm.

Mapping of chl-a in lake Naivasha is strongly influenced by the floating leafed plants (such as Hyacines) which keeps on changing places consistently depending on the wind direction. The application of the best performing algorithm to MERIS data has however enabled us to assess the ecological status of lake Naivasha to some degree of accuracy. Phytoplankton absorption maps of the three cloud free images taken on 20th, 23rd, and 26th of September 2010 were produced using the three band empirical algorithm (Figure 13) and from the three maps it can generally be observed that higher level of chl-a is in the

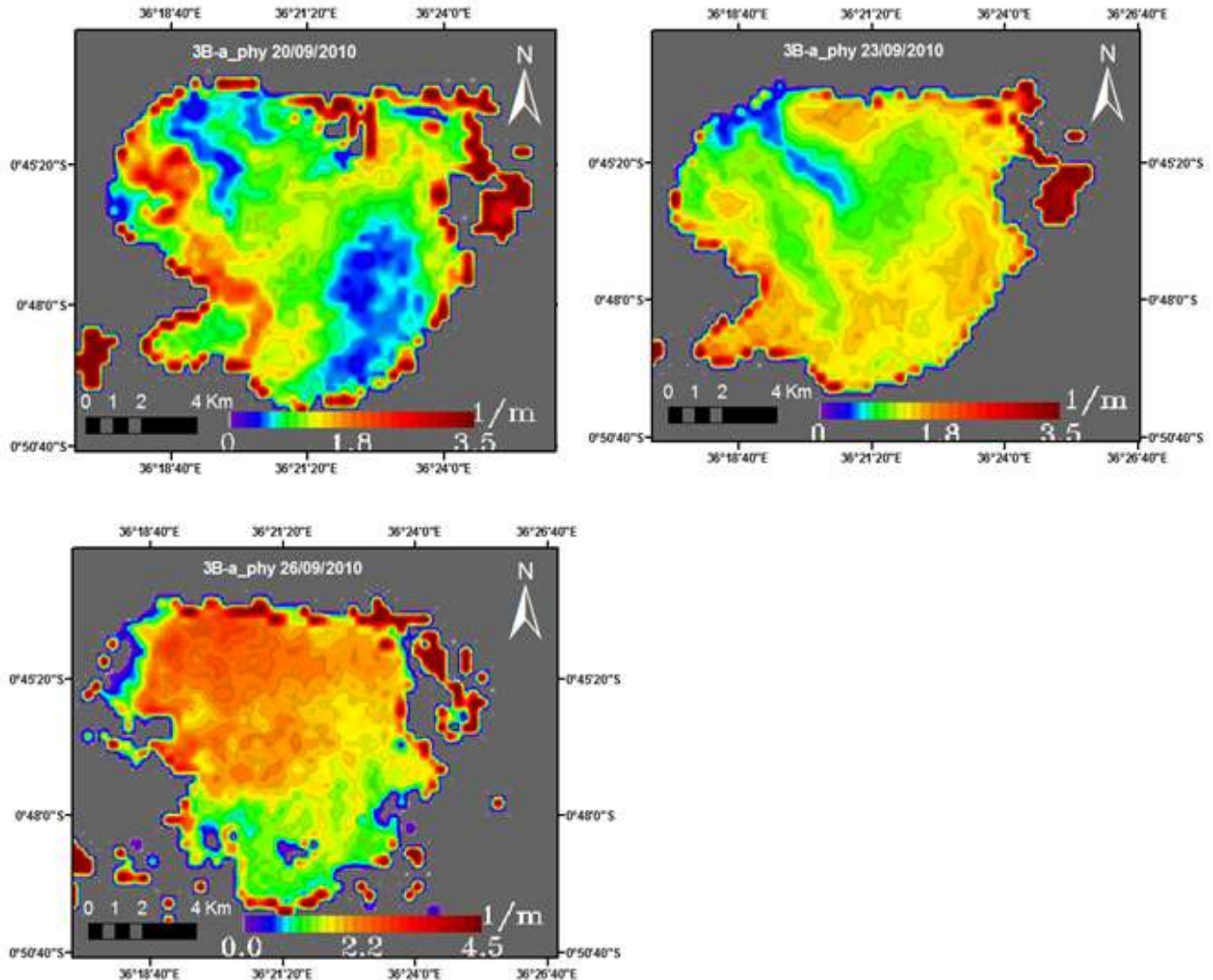


Figure 13. Phytoplankton absorption maps for the 20th, 23rd and 26th of September 2010

The maps indicated are Phytoplankton absorption maps for the 20th, 23rd and 26th of September 2010 computed from the three band model using reflectance in bands 8, 9, and 10. Clouds and land are masked to grey using a threshold in band 13 (865 nm).

Crescent island lagoon, the Hippo point and Lake-Centre (red colour) and the lowest values of chl-a absorption are shown in (blue) on the northern part of the Mennl'e Bay and the Safariland Bay on the 20th and 26th of September 2010 maps. The map on the 23rd of September 2010 also shows lowest value of phytoplankton absorption on the northern part of the Mennel's Bay (blue) though a higher absorption value is mapped on the Safariland bay. This difference could be attributed to the influence of northerly wind blowing from the safariland towards Malewa inlet to collect floating rafts which gave it high chl-a absorption value (red) on the 20th of September 2010. This in turn has left the safariland Bay to lowest chl-a absorption value on the same date.

6. CONCLUSION AND RECOMMENDATION

The study proved that the Medium Resolution Imaging Spectrometer (MERIS) is a very useful tool for studying the distribution of chl-a absorption in a relatively smaller water body such as lake Naivasha. In this work, the three band model by the Gitelson et al; the SCI model and the FLH/MCI algorithms were analyzed for extracting chl-a information in lake Naivasha. Comparison of the three analyzed models revealed that the three band model has a strong linear relationship with the in-situ measured chl-a absorption with high coefficient of determination and low RMSE. It is found that high chl-a level of the lake is beyond the predictive power of the SCI and FLH algorithms. The SCI algorithm initially designed for turbid waters with high SSC was found unfit to retrieve the lake's chl-a level. Despite the high suspended particulate matter observed in the main lake, it is found that the chl-a absorption was higher in the Crescent Island lagoon than in the main lake which was also confirmed by the 3B model. The regression analysis of the model results versus in-situ absorption data reveals that both the SCI and FLH/MCI are inadequate at estimating chl-a from lake Naivasha.

The correlation of index values of the above model with in-situ data provided the basis for the development of retrieval equations and constants for estimating and mapping chl-a absorption coefficient in Lake Naivasha with some degrees of success. However, the use of satellite remote sensing for mapping chl-a absorption coefficients in lake Naivasha is limited by the presence of cloud cover. Despite these problems, satellite data are still preferable over field measurements if one aims to follow the temporal and spatial variation of phytoplankton in the area.

The investigation of temporal variation of the phytoplankton distribution of lake Naivasha, is constrained by the availability of short period remote sensing images which is mainly controlled by the frequent cloud cover in the area.

Comparison of the available satellite data with the in-situ hyperspectral and the laboratory data reveal underlying problems: (i) Comparing data at different spatial and short temporal scales was difficult. In this study, it is observed that a reasonable agreement between measured and model outputs is obtained for the aggregate dataset at a larger spatial scales rather than at shorter spatial and temporal (per every four days) scales where the differences were large and models performed poorly (ii) In situ data suffer from poor reproducibility, related to the natural variability at small spatial scales (patchiness).

The development of new spectral algorithms to account for pigment absorption had varying success in which the 3B model is set with new coefficients of estimating the chl-a content of the lake from RS. The strong correlation of chl-a prediction achieved with 3B model, revealed that empirical algorithms can be used to estimate chl-a information in lake Naivasha accurately.

Though there is a need for comprehensive ground-truth data, the use of remote sensing to monitor algal blooms is beneficial to water managers. Once a comprehensive spectral library is established and validated, models are easily applicable and can rapidly assess pigment concentrations in lake Naivasha.

LIST OF REFERENCES

- Abbott, M. R., Richman, J. G., Letelier, R. M., & Bartlett, J. S. (2000). The spring bloom in the Antarctic Polar Frontal Zone as observed from a mesoscale array of bio-optical sensors. *Deep Sea Research Part II: Topical Studies in Oceanography*, 47(15-16), 3285-3314.
- Ahn, Y.-H., Bricaud, A., & Morel, A. (1992). Light backscattering efficiency and related properties of some phytoplankters. *Deep Sea Research Part A. Oceanographic Research Papers*, 39(11-12), 1835-1855.
- Ahn, Y.-H., & Shanmugam, P. (2006). Detecting the red tide algal blooms from satellite ocean color observations in optically complex Northeast-Asia Coastal waters. [DOI: 10.1016/j.rse.2006.04.007]. *Remote Sensing of Environment*, 103(4), 419-437.
- Aminot, A., & Rey, F. (2000). Standard procedure for the determination of chlorophyll a by spectroscopic methods. *International Council for the Exploration of the Sea* ISSN 0903-2606.
- Anderson, D. M. (2005). *The ecology and oceanography of harmful algal blooms*: United Nations Educational, Scientific and Cultural Organization.
- Babin, M., Morel, A., Claustre, H., Bricaud, A., Kolber, Z., & Falkowski, P. G. (1996). Nitrogen- and irradiance-dependent variations of the maximum quantum yield of carbon fixation in eutrophic, mesotrophic and oligotrophic marine systems. *Deep Sea Research Part I: Oceanographic Research Papers*, 43(8), 1241-1272.
- Bailey, S. W., & Werdell, P. J. (2006). A multi-sensor approach for the on-orbit validation of ocean color satellite data products. *Remote Sensing of Environment*, 102(1-2), 12-23.
- Ballot, A., Kotut, K., Novelo, E., & Krienitz, L. (2009). Changes of phytoplankton communities in Lakes Naivasha and Oloidien, examples of degradation and salinization of lakes in the Kenyan Rift Valley. *Hydrobiologia*, 632(1), 359-363.
- Becht, R., & Harper, D. M. (2002). Towards an understanding of human impact upon the hydrology of Lake Naivasha, Kenya. *Hydrobiologia*, 488(1), 1-11.
- Binding, C. E., Bowers, D. G., & Mitchelson-Jacob, E. G. (2004). Estimating suspended sediment concentrations from ocean colour measurements in moderately turbid waters; the impact of variable particle scattering properties. *Remote Sensing of Environment*, 94(2005), 373-383.
- Dall'Olmo, G., & Gitelson, A. A. (2005a). Effect of bio-optical parameter variability on the remote estimation of chlorophyll-a concentration in turbid productive waters: experimental results. *Appl. Opt.*, 44(3), 412-422.
- Dall'Olmo, G., & Gitelson, A. A. (2005b). Effect of bio-optical parameter variability on the remote estimation of chlorophyll-a concentration in turbid productive waters: experimental results - erratum. *Appl. Opt.*, 44(16), 3342-3342.
- Dall'Olmo, G., & Gitelson, A. A. (2006). Effect of bio-optical parameter variability and uncertainties in reflectance measurements on the remote estimation of chlorophyll-a concentration in turbid productive waters: modeling results. *Appl. Opt.*, 45(15), 3577-3592.
- Dekker, A. G., Malthus, T. J., & Seyhan, E. (1991). Quantitative modeling of inland water quality for high-resolution MSS systems. *Geoscience and Remote Sensing, IEEE Transactions on*, 29(1), 89-95.
- Dekker, A. G. (2003). *Seagrass change assessment using satellite data for Wallis Lake, NSW [electronic resource] : a consultancy report to the Great Lakes Council and Department of Land and Water Conservation / Environmental Remote Sensing Group, Arnold G. Dekker, Janet M. Anstee and Vittorio E. Brando*. Canberra :: CSIRO Land and Water.
- Doxaran, D., Cherukuru, N., & Lavender, S. J. (2006). Apparent and inherent optical properties of turbid estuarine waters: measurements, empirical quantification relationships, and modeling. *Appl. Opt.*, 45(10), 2310-2324.
- Everard, M., & Harper, D. M. (2002). Towards the sustainability of the Lake Naivasha Ramsar site and its catchment. *Hydrobiologia*, 488(1), 191-203.
- Gilerson, A., Zhou, J., Hlaing, S., Ioannou, I., Schalles, J., Gross, B., Moshary, F., & Ahmed, S. (2007). Fluorescence component in the reflectance spectra from coastal waters. Dependence on water composition. *Opt. Express*, 15(24), 15702-15721.
- Gitelson. (1992). The peak near 700nm on radiance spectra of algae and water : relationships of its magnitude and position with chlorophyll concentration. *Int. J. Remote Sens.*, 13(17), 3367-3373.
- Gitelson, A., Szilagyi, F., & Mittenzwey, K. H. (1993). Improving quantitative remote sensing for monitoring of inland water quality. *Water Research*, 27(7), 1185-1194.

- Gitelson, A. A., Buschmann, C., & Lichtenthaler, H. K. (1999). The Chlorophyll Fluorescence Ratio F735/F700 as an Accurate Measure of the Chlorophyll Content in Plants. *Remote Sensing of Environment*, 69(3), 296-302.
- Gitelson, A. A., Dall'Olmo, G., Moses, W., Rundquist, D. C., Barrow, T., Fisher, T. R., Gurlin, D., & Holz, J. (2008). A simple semi-analytical model for remote estimation of chlorophyll-a in turbid waters: Validation. [doi: DOI: 10.1016/j.rse.2008.04.015]. *Remote Sensing of Environment*, 112(9), 3582-3593.
- Gitelson, A. A., Laorawat, S., Keydan, G. P., & Vonshak, A. (1995). OPTICAL PROPERTIES OF DENSE ALGAL CULTURES OUTDOORS AND THEIR APPLICATION TO REMOTE ESTIMATION OF BIOMASS AND PIGMENT CONCENTRATION IN SPIRULINA PLATENSIS (CYANOBACTERIA)1. *Journal of Phycology*, 31(5), 828-834.
- Gitelson, A. A., Schalles, J. F., & Hladik, C. M. (2007). Remote chlorophyll-a retrieval in turbid, productive estuaries: Chesapeake Bay case study. *Remote Sensing of Environment*, 109(4), 464-472.
- Gons, H. J. (1999). Optical Teledetection of Chlorophyll a in Turbid Inland Waters. *Environmental Science & Technology*, 33(7), 1127-1132.
- Gons, H. J., Burger-Wiersma, T., Otten, J., & Rijkeboer, M. (1992). Coupling of phytoplankton and detritus in a shallow, eutrophic lake (Lake Loosdrecht, The Netherlands). *Hydrobiologia*, 233(1), 51-59.
- Gons, H. J., Rijkeboer, M., & Ruddick, K. G. (2002). A chlorophyll-retrieval algorithm for satellite imagery (Medium Resolution Imaging Spectrometer) of inland and coastal waters. *J. Plankton Res.*, 24(9), 947-951.
- Gordon, H. R., Brown, O. B., & Jacobs, M. M. (1975). Computed Relationships Between the Inherent and Apparent Optical Properties of a Flat Homogeneous Ocean. *Appl. Opt.*, 14(2), 417-427.
- Gordon, H. R., Clark, D. K., Brown, J. W., Brown, O. B., Evans, R. H., & Broenkow, W. W. (1983). Phytoplankton pigment concentrations in the Middle Atlantic Bight: comparison of ship determinations and CZCS estimates. *Optical Society of America.*, 22(1).
- Gower, King, S., Borstad, G., & Brown, L. (2005). Detection of intense plankton blooms using the 709 nm band of the MERIS imaging spectrometer. *International Journal of Remote Sensing*, 26(9), 2005–2012.
- Gower, J., King, S., Borstad, G., & Brown, L. (2005). Detection of intense plankton blooms using the 709 nm band of the MERIS imaging spectrometer. *International Journal of Remote Sensing*, 26(9), 2005–2012.
- Gower, J. F. R., Brown, L., & Borstad, G. A. (2004). Observation of chlorophyll fluorescence in west coast waters of Canada using the MODIS satellite sensor. *J. Remote Sensing*, 30(1), 17–25.
- Guanter, L., Ruiz-Verdú, A., Odermatt, D., Giardino, C., Simis, S., Estellés, V., Heege, T., Domínguez-Gómez, J. A., & Moreno, J. (2010). Atmospheric correction of ENVISAT/MERIS data over inland waters: Validation for European lakes. *Remote Sensing of Environment*, 114(3), 467-480.
- Han, L., & Rundquist, D. C. (1997). Comparison of NIR/RED ratio and first derivative of reflectance in estimating algal-chlorophyll concentration: A case study in a turbid reservoir. *Remote Sensing of Environment*, 62(3), 253-261.
- Han, L., Rundquist, D. C., Liu, L. L., Fraser, R. N., & Schalles, J. F. (1994). 'The spectral responses of algal chlorophyll in water with varying levels of suspended sediment'. *International Journal of Remote Sensing*, 15(18), 3707 — 3718.
- Harper, D. M., Adams, C., & Mavuti, K. (1995). The aquatic plant communities of the Lake Naivasha wetland, Kenya: pattern, dynamics and conservation. *Wetlands Ecology and Management*, 3(2), 111-123.
- Harper, D. M., Mavuti, K. M., & Muchiri, S. M. (1990). Ecology and Management of Lake Naivasha, Kenya, in Relation to Climatic Change, Alien Species' Introductions, and Agricultural Development. [10.1017/S037689290003277X]. *Environmental Conservation*, 17(04), 328-336.
- Harper, M. D. (1992). The ecological relationships of aquatic plants at Lake Naivasha, Kenya. *Hydrobiologia*, 232(1), 65-71.
- Hoge, F. E., Lyon, P. E., Swift, R. N., Yungel, J. K., Abbott, M. R., Letelier, R. M., & Esaias, W. E. (2003). Validation of Terra-MODIS Phytoplankton Chlorophyll Fluorescence Line Height. I. Initial Airborne Lidar Results. *Appl. Opt.*, 42(15), 2767-2771.
- Hubble, D. S., & Harper, D. M. (2002a). Nutrient control of phytoplankton production in Lake Naivasha, Kenya. *Hydrobiologia*, 488(1), 99-105.
- Hubble, D. S., & Harper, D. M. (2002b). Nutrient control of phytoplankton production in Lake Naivasha, Kenya. *Hydrobiologia*, 488, 99-105.

- Janssen, M. A., & Carpenter, S. R. (1999). Managing the Resilience of Lakes: A Multi-agent Modeling Approach. *Ecology and Society*, 3(2), 15.
- Jupp, D., Kirk, J., & Harris, G. (1994). Detection, identification and mapping of cyanobacteria — Using remote sensing to measure the optical quality of turbid inland waters. *Marine and Freshwater Research*, 45(5), 801-828.
- Kebede, G. A. (2011). Remote sensing of suspended particulate matters in lake Naivasha, Kenya. *unpublished*, 1(1), 50.
- Kutser, T., Metsamaa, L., Strömbeck, N., & Vahtmäe, E. (2006). Monitoring cyanobacterial blooms by satellite remote sensing. [DOI: 10.1016/j.ecss.2005.11.024]. *Estuarine, Coastal and Shelf Science*, 67(1-2), 303-312.
- Laney, S. R., Letelier, R. M., & Abbott, M. R. (2005). Parameterizing the natural fluorescence kinetics of *Thalassiosira weissflogii*. *Limnol. Oceanogr*, 50(5), 1499–1510.
- Lee, Z., Carder, K., Arnone, R., & He, M. (2007). Determination of Primary Spectral Bands for Remote Sensing of Aquatic Environments. *sensors*, 7, 3428-3441.
- Lorenzen, C. J. (1966). A method for the continuous measurement of in vivo chlorophyll concentration. *Deep Sea Research and Oceanographic Abstracts*, 13(2), 223-227.
- Metsamaa, L., Kutser, T., & Strombeck, N. (2006). Recognising cyanobacterial blooms based on their optical signature: a modelling study. [Article]. *Boreal Environment Research*, 11(6), 493-506.
- Mironga, J. M. (2006). The effect of water Hyacinth, Eichhornia Crassipes, infestation on phytoplankton productivity in Lake Naivasha and the status of control.
- Mitchell, B. G., Kahru, M., Wieland, J., & Stramska, M. (2002). Determination of spectral absorption coefficients of particles, dissolved material and phytoplankton for discrete water samples. In O. o. p. f. s. o. c. s. validation (Ed.), (Vol. 2, pp. 231–257).
- Mittenzwey, K.-H., Ullrich, S., Gitelson, A. A., & Kondratiev, K. Y. (1992). Determination of Chlorophyll a of inland waters on the basis of spectral reflectance. *Limnology and Oceanography* 37(1), 147-149.
- Moore, G. F., Aiken, J. a., & Lavender, S. J. (1999). The atmospheric correction of water colour and the quantitative retrieval of suspended particulate matter in Case II waters: application to MERIS. *International Journal of Remote Sensing*, 20.
- Morel, A., & Bélanger, S. (2006). Improved detection of turbid waters from ocean color sensors information. *Remote Sensing of Environment*, 102(3-4), 237-249.
- Morel, A., & Gentili, B. (1991). Diffuse reflectance of oceanic waters: its dependence on Sun angle as influenced by the molecular scattering contribution. *Appl. Opt.*, 30(30), 4427-4438.
- Morel, A., & Gordon, H. R. (1980). Report of the Working Group on Water Color. *Boundary-Layer Meteorology*, 18, 343-355.
- Moses, W. J., Gitelson, A. A., Berdnikov, S., & Povazhnyy, V. (2009). Estimation of chlorophyll- a concentration in case II waters using MODIS and MERIS data—successes and challenges. *Environmental Research Letters*, 4(4), 045005.
- Pope, R. M., & Fry, E. S. (1997). Absorption spectrum ~380–700 nm of pure water. II. Integrating cavity measurements. *APPLIED OPTICS*, 36(33).
- Randolph, K., Wilson, J., Tedesco, L., Li, L., Pascual, D. L., & Soyeux, E. (2007, submitted). Remote Sensing of Cyanobacteria in turbid productive water using optically active pigments, chlorophyll a and phycocyanin. *Submitted*.
- Reinart, A., & Kutser, T. (2006). Comparison of different satellite sensors in detecting cyanobacterial bloom events in the Baltic Sea. *Remote Sensing of Environment*, 102(1-2), 74-85.
- Rowan, K. (1989). *Photosynthetic pigments of algae*. Cambridge University Press.
- Salama, M. S., & Shen, F. (2010). Simultaneous atmospheric correction and quantification of suspended particulate matters from orbital and geostationary earth observation sensors. [DOI: 10.1016/j.ecss.2009.10.001]. *Estuarine, Coastal and Shelf Science*, 86(3), 499-511.
- Schalles, J. F., Gitelson, A. A., Yacobi, Y. Z., & Kroenke, A. E. (1998). Estimation Of Chlorophyll a From Time Series Measurements Of High Spectral Resolution Reflectance In an Eutrophic Lake. *Journal of Phycology*, 34(2), 383-390.
- Shen, F., Zhou, Y.-X., Li, D., Zhu, W., & Salama, M. (2010). MERIS estimation of chlorophyll-a concentration in the turbid sediment-laden waters of the Changjiang (Yangtze) Estuary. [Journal]. *International Journal of Remote Sensing*, 19.
- Siegel, D. A., Wang, M., Maritorena, S., & Robinson, W. (2000). Atmospheric Correction of Satellite Ocean Color Imagery: The Black Pixel Assumption. *Appl. Opt.*, 39(21), 3582-3591.
- Simis, S. G. H., Tijdens, M., Hoogveld, H. L., & Gons, H. J. (2005). Optical changes associated with cyanobacterial bloom termination by viral lysis. *Journal of Plankton Research*, 27(9), 937-949.

- Vermote, E. F., El Saleous, N. Z., & Justice, C. O. (2002). Atmospheric correction of MODIS data in the visible to middle infrared: first results. *Remote Sensing of Environment*, 83(1-2), 97-111.
- Vos, R. J., Hakvoortb, J. H. M., Jordansb, R. W. J., & Ibelingsc, B. W. (2003). Multiplatform optical monitoring of eutrophication in temporally and spatially variable lakes. *The Science of the Total Environment*, 312(2003), 221-243.
- Yacobi, Y. Z., Gitelson, A., & Mayo, M. (1995). Remote sensing of chlorophyll in Lake Kinneret using highspectral-resolution radiometer and Landsat TM: spectral features of reflectance and algorithm development [Life Science]. *Journal of Phytoplankton Research*, 17(11), 2155-2173.
- Zhao, J., Cao, W., Yang, Y., Wang, G., Zhou, W., & Sun, Z. (2008). Measuring natural phytoplankton fluorescence and biomass: A case study of algal bloom in the Pearl River estuary. []. *Marine Pollution Bulletin*, 56(10), 1795-1801.

APPENDIX

MERIS wavelength	20-Sep-10			23-Sep-10			26-Sep-10		
	RMSE	rho path	Tv	RMSE	rho path	Tv	RMSE	rho path	Tv
412.6910	0.00181	0.04237	1.00000	0.00109	0.04360	1.00000	0.00244	0.04690	0.53833
442.5590	0.00168	0.03266	1.00000	0.00116	0.03366	1.00000	0.00232	0.03517	0.73705
489.8820	0.00161	0.02140	1.00000	0.00139	0.02265	1.00000	0.00220	0.02136	1.00000
509.8190	0.00159	0.01722	1.00000	0.00155	0.01872	1.00000	0.00207	0.02297	0.62951
559.6940	0.00174	0.00880	1.00000	0.00209	0.01137	1.00000	0.00192	0.02041	0.52423
619.6010	0.00172	0.00574	1.00000	0.00264	0.00748	1.00000	0.00194	0.00651	1.00000
664.5731	0.00181	0.00523	1.00000	0.00268	0.00690	1.00000	0.00185	0.00598	1.00000
680.8210	0.00186	0.00501	1.00000	0.00260	0.00634	1.00000	0.00195	0.00581	1.00000
708.3290	0.00244	0.00353	1.00000	0.00276	0.00600	1.00000	0.00236	0.00423	1.00000
753.3710	0.00223	0.00553	1.00000	0.00171	0.00772	1.00000	0.00551	0.00787	1.00000
778.4091	0.00222	0.00490	1.00000	0.00176	0.00722	1.00000	0.00583	0.00741	1.00000
864.8760	0.00188	0.00431	1.00000	0.00115	0.00635	1.00000	0.00674	0.00715	1.00000
884.9444	0.00177	0.00391	1.00000	0.00099	0.00592	1.00000	0.00694	0.00690	1.00000
900.0001	0.00165	0.00130	1.00000	0.00076	0.00332	1.00000	0.00491	0.00389	1.00000